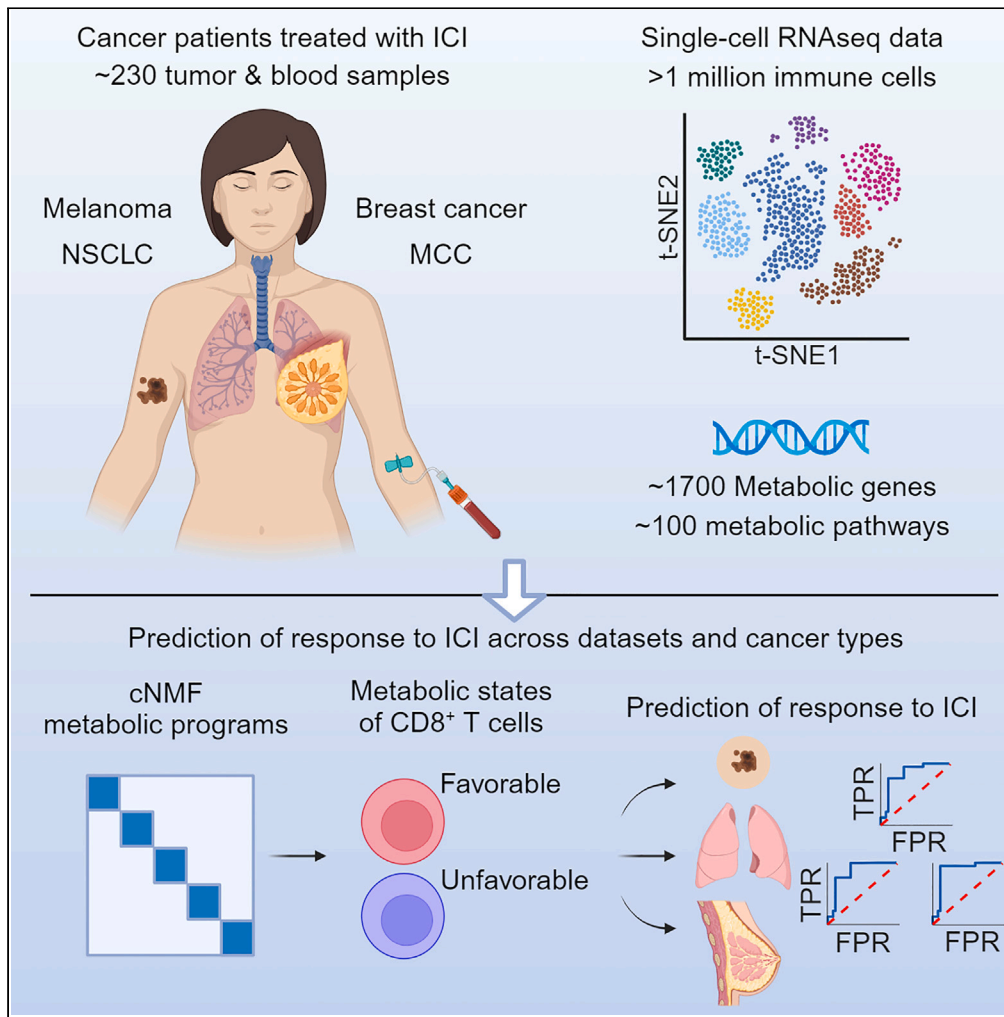**Article**

Metabolic predictors of response to immune checkpoint blockade therapy

Ofir Shorer, Keren Yizhak

kyizhak@technion.ac.il

Highlights

Immune cells in the tumor microenvironment show metabolic heterogeneity

CD8^{+} T cells with similar immunological state can demonstrate metabolic differences

A metabolic gene signature is capable of predicting patient response to ICI

A unique tumor metabolic signature contributes to acquired ICI resistance

Article

Metabolic predictors of response to immune checkpoint blockade therapy

Ofir Shorer[1] and Keren Yizhak[1,2,3,*]

SUMMARY

Metabolism of immune cells in the tumor microenvironment (TME) plays a critical role in cancer patient response to immune checkpoint inhibitors (ICI). Yet, a metabolic characterization of immune cells in the TME of patients treated with ICI is lacking. To bridge this gap we performed a semi-supervised analysis of ~1700 metabolic genes using single-cell RNA-seq data of > 1 million immune cells from ~230 samples of cancer patients treated with ICI. When clustering cells based on their metabolic gene expression, we found that similar immunological cellular states are found in different metabolic states. Most importantly, we found metabolic states that are significantly associated with patient response. We then built a metabolic predictor based on a dozen gene signature, which significantly differentiates between responding and non-responding patients across different cancer types (AUC = 0.8–0.92). Taken together, our results demonstrate the power of metabolism in predicting patient response to ICI.

INTRODUCTION

Over the past decade cancer therapy has been revolutionized by the usage of immune checkpoint inhibitors (ICI), resulting in unprecedented rates of long-lasting tumor responses in patients with a variety of cancers.[1] Nevertheless, most patients do not respond to treatment or acquire resistance,[2,3] reaching response rates of less than 40% in solid tumors[4] with a large number of partial responders.[5] To address this challenge, multiple biomarkers of response have been suggested, including different gene signatures,[6–8] T cell abundance levels,[9–11] as well as metrics related to the tumor's genetics, including the tumor mutational burden and copy number alteration.[12–16] These and other metrics are, however, rarely predictive across datasets, and certainly across different cancer types.

More recently, differences in the metabolic adaptation of tumor and immune cells and their competition for resources have been shown to contribute to patient response.[17–20] Alterations in cellular metabolism lead to tumor-immune interactions that simultaneously deplete vital nutrients from the common environment and produce immunosuppressive metabolic byproducts.[20,21] For instance, enzymatic activation of IDO depletes tryptophan levels, a vital nutrient for T cell response. At the same time, this activity generates kynurenine, a metabolite causing upregulation of PD1 on activated CD8$^+$ T cells.[22,23] Another example involves the high lactate levels generated by tumor cells due to up-regulation of lactate dehydrogenase (LDH), resulting in an acidic environment that suppresses natural killer (NK) cells cytotoxicity, blocks monocytes and dendritic cells differentiation, and inhibits effector T cells activity.[24–27] These and other findings were mainly established in *in vitro* systems or in animal models. Studying the metabolic transcriptomic changes that occur in immune cells found in the TME of patients treated with ICI, can therefore shed light on mechanisms of response to therapy and highlight immune metabolic vulnerabilities.

Here, we perform a semi-supervised analysis of single-cell RNA-seq data from tumor biopsies of patients treated with ICI, focusing on ~1700 metabolic genes that are associated with ~100 metabolic pathways.[28] Focusing on this well-defined cellular process and its narrowed gene set, enabled us to discover novel associations with patient response that were masked under the genome-wide analyses. We found that different immune cell states share similar metabolic activity and vice versa, resulting in a novel classification to cellular states, mainly involving CD8$^+$ T cells. Furthermore, we detected metabolic clusters that are significantly associated with patient response. A non-discrete analysis of metabolic programs revealed a metabolic gene signature that is significantly associated with tumor progression or regression across various cancer types, including melanoma, Merkel cell carcinoma (MCC), lung, and breast cancers. Finally, we show a metabolic involvement in the polarization of macrophages to a suppressive M2-like phenotype in an acquired resistance patient, together with the associated tumor metabolic changes.

RESULTS

Immune cellular metabolism and its association with patient response to ICI

To identify immune metabolic changes at the single-cell level and study their association with ICI treatment and patient response, we re-analyzed our previously published dataset that includes single-cell RNA sequencing (scRNA-seq) of 16,291 CD45$^+$ cells from 48 tumor

[1]Department of Cell Biology and Cancer Science, The Ruth and Bruce Rappaport Faculty of Medicine, Technion - Israel Institute of Technology, Haifa 3525422, Israel
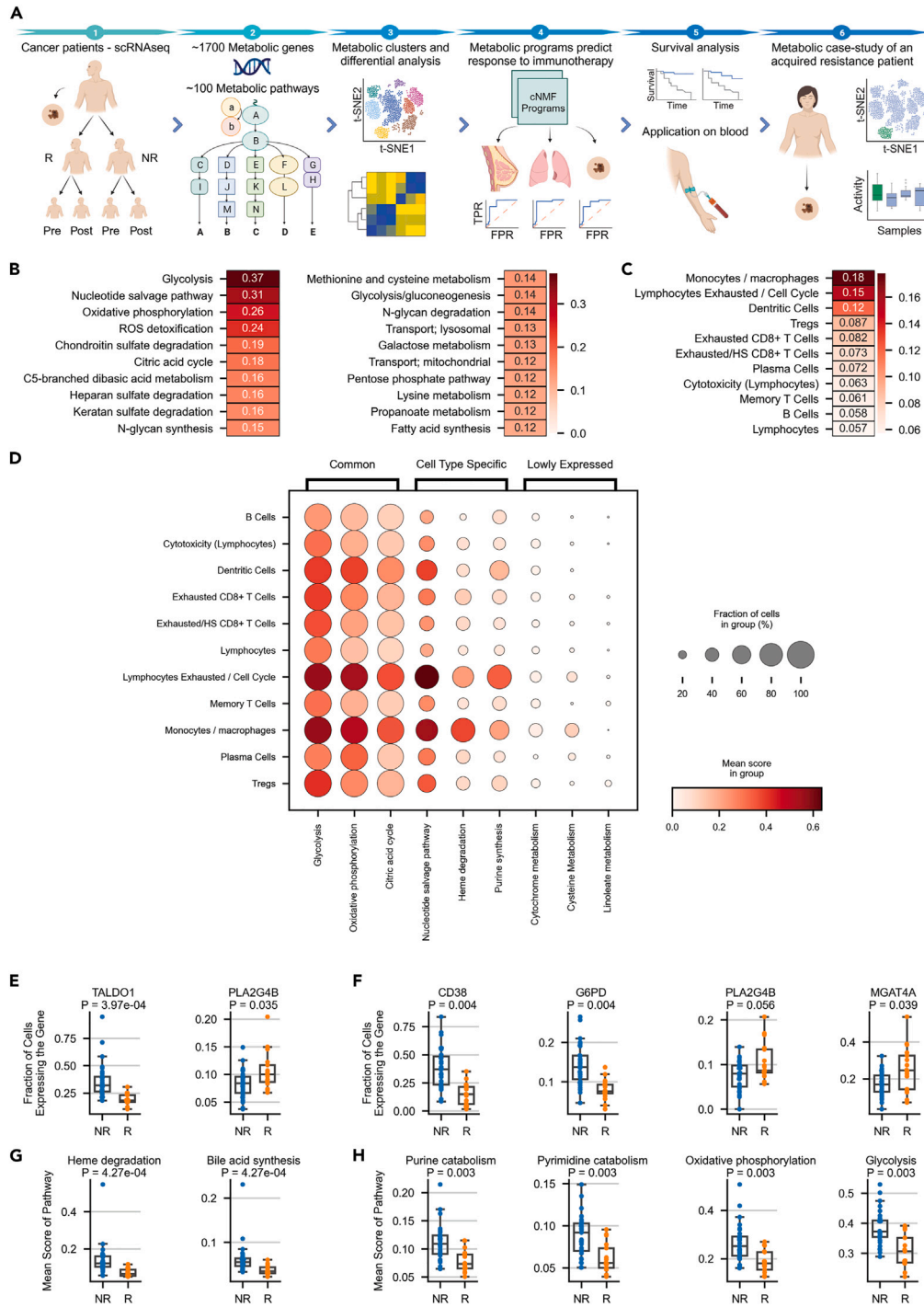[2]The Taub Faculty of Computer Science, Technion - Israel Institute of Technology, Haifa 3200003, Israel
[3]Lead contact
*Correspondence: kyizhak@technion.ac.il
https://doi.org/10.1016/j.isci.2023.108188

Figure 1. Immune cellular metabolism and its association with patient response to ICI

(A) Schematic workflow of the study.

(B) Top 20 active metabolic pathways across all single-cells, colored by the mean score of each pathway across all single-cells.

(C) Rank of metabolic activity by immune cell types, colored by the mean score of all metabolic pathways in each cell type.

(D) Selected metabolic pathways and their mean scores across different cell types separated by commonly expressed, cell-type specific, and lowly expressed pathways.

(E) Fraction of cells expressing metabolic genes associated with patient response across all cells within each sample. Wilcoxon rank sum test.

Figure 1. *Continued*

(F) Fraction of cells expressing metabolic genes associated with patient response across CD8^{+} T cells within each sample. Wilcoxon rank sum test.

(G) Mean score of metabolic pathways associated with non-responding samples across all cells within each sample. Wilcoxon rank sum test.

(H) Mean score of metabolic pathways associated with non-responding samples across CD8^{+} T cells within each sample. Wilcoxon rank sum test. Abbreviations: R = Responders, NR = Non-responders. See also Figures S1 and S2 and Table S3.

biopsies taken from 32 stage IV metastatic melanoma patients treated with ICI[29] (Table S1). Eleven patients had longitudinal biopsies and 20 patients with one or two biopsies, taken either at baseline or during treatment. Tumor samples were classified based on radiologic assessments into progression/non-responder (NR; n = 31, including stable disease (SD)/progressive disease (PD) samples) or regression/responder (R; n = 17, including complete response (CR)/partial response (PR) samples).[30] Using the previously defined cell classification into 11 clusters,[29] we devised a score for 97 metabolic pathways based on the expression of their associated metabolic genes[28] (Table S2, STAR Methods).

This analysis showed several metabolic pathways which are significantly more expressed than others across all cells, as well as specific cell types and states that are more metabolically active (Figures 1B, 1C, and S1). Specifically, we found that pathways such as glycolysis, oxidative phosphorylation (OXPHOS), and tricarboxylic acid (TCA) cycle, are generally active across many cell types with heterogeneous pattern of activation, as was similarly demonstrated in melanoma and in head and neck squamous cell carcinoma (HNSCC) patients.[31] In contrast, other pathways such as nucleotide salvage pathway, heme degradation, and purine synthesis, are active only in specific cell types (Figure 1D). Moreover, we found that cells from the myeloid lineage and cycling exhausted T cells, that were previously associated with negative response to immunotherapy,[29] are the most metabolically active. On the other hand, memory T cells and B cells that were previously associated with positive response to immunotherapy,[29] show lower metabolic expression across all pathways (Figure 1C). Overall, this continuous metabolic score showed high heterogeneity across cell types, going beyond sequencing reading depth (Figure S2).

Examining the association between metabolic genes and patient response to ICI, we found a couple of genes that are significantly up-regulated in responding samples (*PLA2G4B* and *DGKD*), both are involved in glycerophospholipid metabolism (Figure 1E; Table S3). This pathway was shown to be involved in different immune cellular functions, including T cell proliferation and activation, and macrophages differentiation.[32–34] Additional genes were found to be significantly up-regulated in non-responding samples, including glycolytic genes (*PGAM1*, *GPI*, *TPI1*, *ENO1*, *GAPDH*), pentose phosphate pathway genes (*TALDO1*, *G6PD*), TCA cycle genes (*IDH2*, *MDH2*), and oxidative phosphorylation genes (*NDUFA9*, *NDUFA12*, *UQCRFS1*, *NDUFA13*, *NDUFB4*, *COX5B*, Figure 1E; Table S3). When focusing only on CD8^{+} T cells, the N-glycosylation enzyme *MGAT4A* and *PLA2G4B* were significantly expressed in responders, while *GAPDH*, *G6PD*, *CD38*, *MDH2*, *DBI* and others, were significantly expressed in non-responders (Figure 1F; Table S3). At the pathway level, while no metabolic pathways were found to be significantly expressed in responding samples, in non-responding samples we saw a significant expression of pathways such as heme degradation, bile acid synthesis, purine catabolism, oxidative phosphorylation, fatty acid oxidation (FAO), and glycolysis (Figure 1G; Table S3). Repeating the pathway analysis using only CD8^{+} T cells, we found a significant expression of multiple pathways including purine catabolism, glycolysis, OXPHOS, and pyrimidine catabolism in non-responding samples (Figure 1H; Table S3). Of note, as previously found in the genome-wide analysis,[29] no significant metabolic changes were found between baseline and post-treatment samples. Overall, our analysis identified specific cell states that are more metabolically active, and metabolic gene markers associated with regression or progression of individual tumors in response to ICI therapy.

Metabolic-based clusters of melanoma infiltrated immune cells and their association with patient response to ICI

To metabolically define the different immune cells in an unbiased manner, we clustered all ∼16,000 cells using the pre-defined set of 1689 metabolic genes[28] (Table S2). This process yielded 10 distinct metabolic clusters that are partially different from the 11 original clusters obtained using all genes (Figures 2A and 2B; Table S3). Specifically, the previously defined clusters of B and plasma-cells (C5 and C9), cycling cells (C6), and myeloid cells (C7, C8 and C10), were also found to have a distinct metabolic signature (Figures 2B and S3; Table S3): C5 significantly expressed genes related to lipid and glycan metabolism, such as *PLCG2*, *ALOX5*, *PIK3C2B*, *ST6GAL1*, and *MGAT5*; C6 was enriched with genes of OXPHOS, TCA cycle, and FAO, as well as genes related to nucleotide interconversion (*RRM1*, *RRM2*, *DUT*, *TK1*, *TYMS*) and genes involved in folate metabolism (*DHFR*, *GGH*, *MTHFD1* and *FPGS*), all contribute to cell proliferation. Macrophages were divided into two metabolic clusters (C7 and C8), where C8 demonstrated a general upregulation of metabolic pathways compared to C7, including OXPHOS, TCA cycle, metabolism of fructose and mannose, pyrimidine synthesis, cholesterol metabolism, and phosphatidylinositol phosphate metabolism (Table S3). When comparing the two clusters at the gene level, C8 significantly expressed genes related to its enriched metabolic pathways, including apolipoproteins (*APOC1*, *APOC2*, *APOE*), OXPHOS genes (NDUF genes, COX genes and *CYC1*), and TCA cycle genes (*IDH1*, *MDH1*, *SDHA*, *SDHB*, *SDHD*, and *FH*), while C7 expressed more *IDO1*, *AGPAT9*, *SDS*, and others (Table S3).

Unlike these metabolic clusters that corresponded to known immune cell types, each of the metabolic clusters C1-C4 was comprised a mixture of T cells states, including cytotoxic, exhausted and memory (Figures 2A and 2B). This finding demonstrates that different immunological states can share metabolic similarity and vice versa. To examine if any of these clusters is associated with patient response, we quantified the fraction of cells in each sample and in each metabolic cluster. We found seven clusters as significantly abundant in one of the response groups (Figure 2C). Two of them, C2 and C3, were among the newly defined metabolic clusters, such that C2 was found to be more abundant in non-responders (two-sided Wilcoxon rank sum p value = 0.009) and C3 was more abundant in responders (two-sided Wilcoxon rank sum p value = 0.009). Comparing the two clusters, C2 was enriched with glycolytic genes (*TPI1*, *PGAM1*, *PKM*, *LDHB*, *GPI*), OXPHOS genes from the cytochrome *c* oxidase and NADH dehydrogenases complexes, as well as antioxidant genes such as *SOD1*, *PRDX1*, *PRDX2*, and *PRDX3*. On the other hand, C3 was characterized by a general down-regulation of metabolic genes (Table S3; Figure S3).
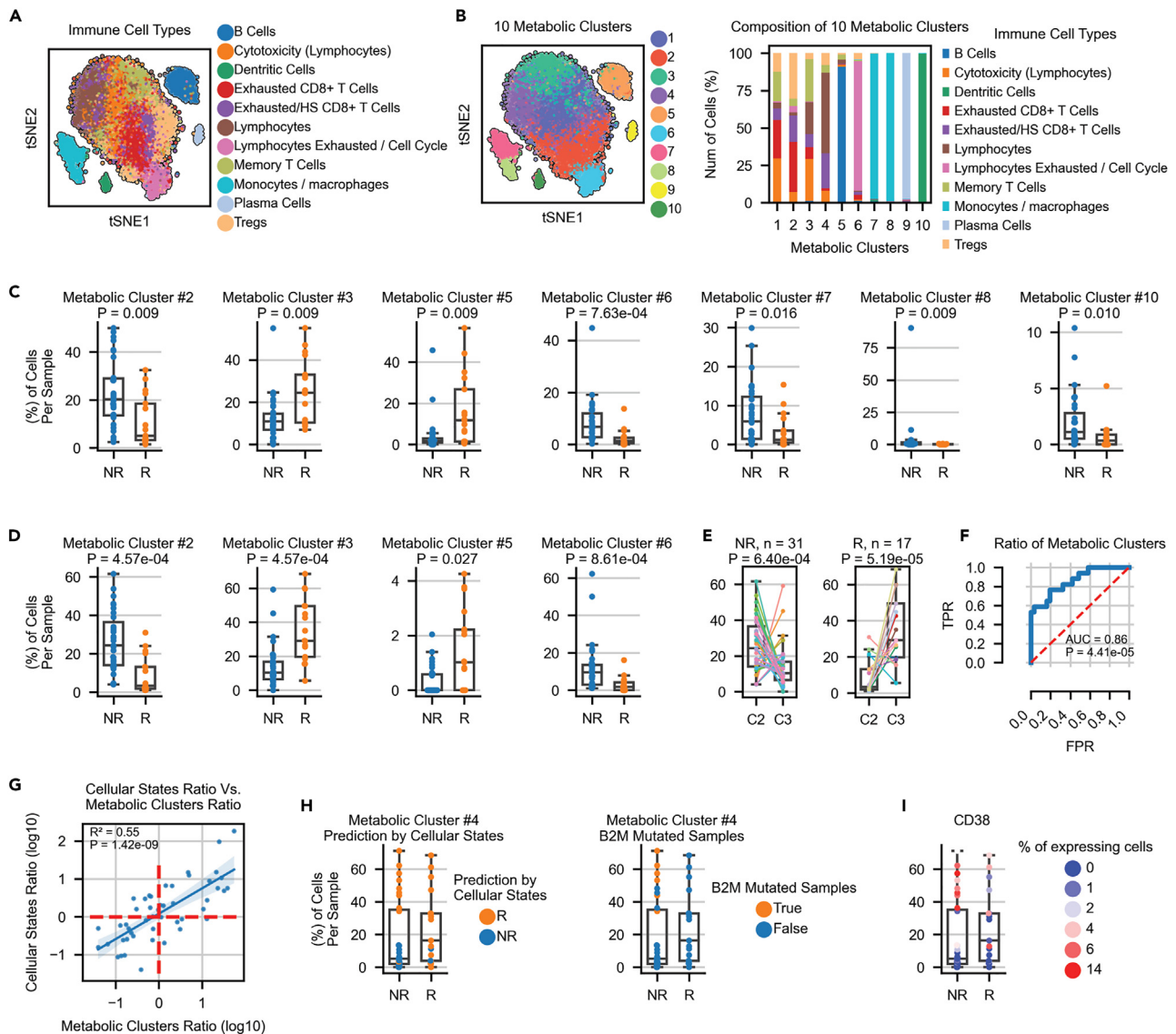
Figure 2. Metabolic-based clusters of melanoma infiltrated immune cells and their association with patient response to ICI

(A) Classification of CD45^{+} cells to different types and cellular states according to Sade-Feldman et al.[29]

(B) Metabolic clusters of immune cells (left) and their composition by immune cell-types (right).

(C) Percentage of immune cells found in metabolic clusters associated with patient response, separated by their response status. Wilcoxon rank sum test.

(D) Percentage of CD8^{+} T cells found in metabolic clusters associated with patient response, separated by their response status. Wilcoxon rank sum test.

(E) Abundance of CD8^{+} T cells from metabolic clusters C2 and C3 in each sample by the two response groups. Wilcoxon rank sum test.

(F) The predictive power for response of the metabolic score calculated as the ratio of CD8^{+} T cells from C3 and C2 in each sample. Wilcoxon rank sum test.

(G) Spearman correlation between the metabolic score of each sample vs. the predictive score suggested by our previous study.[29]

(H) High abundance of CD8^{+} T cells from C4 in the misclassified non-responders (left), including B2M mutated samples (right), and their response prediction according to the immunological predictor of Sade-Feldman et al.[29]

(I) The abundance of CD8^{+} T cells from C4 in each sample colored according to the fraction of memory-activated CD8^{+} T cells in C4 that express *CD38*, out of the total number of CD8^{+} T cells in each sample. See also Figures S3–S5, as well as Table S3.

This finding corresponds to the general downregulation of metabolic pathways seen in cell types associated with responding samples (Figure 1C). When we compared the two clusters at the level of metabolic pathways, C2 was enriched with pathways such as OXPHOS, TCA cycle, glycolysis, and pentose phosphate pathway, while C3 had no significant enrichment of metabolic pathways (Table S3). No significant difference between baseline and post-therapy samples was detected in any of the metabolic clusters, in similar to our previous report on the genome-wide clusters.[29] Finally, a trajectory analysis demonstrated the metabolic transition from a favorable metabolic cluster (C3), toward an unfavorable metabolic cluster (C2), eventually reaching to cluster C6, which has properties of terminal exhaustion[29] (Figure S4). Overall, our

semi-supervised analysis that was focused only on metabolic genes, detected a sub-classification of known immunological T cell states, and identified metabolic clusters and genes that were not previously associated with patient response to ICI.

A metabolic classification of CD8$^+$ T cells is predictive of patient response to ICI

Based on the high abundance of CD8$^+$ T cells in the clusters associated with patient response, and their role in recognizing tumor antigens, we next focused our analysis on the metabolism of 6350 CD8$^+$ T cells found in this dataset.[29] Examining their fraction in the clustering groups C2 and C3, we observed the same direction of association with patient response, but with a higher significance level (two-sided Wilcoxon rank sum p value = $4.57*10^{-4}$ for both clusters, Figure 2D). Notably, the two metabolic states co-existed in all samples, such that per sample, C2 was generally more abundant in non-responders (two-sided Wilcoxon rank sum p value = $6.4*10^{-4}$) and C3 was more abundant in responders (two-sided Wilcoxon rank sum p value = $5.19*10^{-5}$) (Figure 2E). Classifying samples as responders or non-responders based on C3/C2 ratios achieved high predictive power (area under the curve [AUC] of receiver operating characteristic [ROC] = 0.86, n = 48; two-sided Wilcoxon rank sum p value = $4.41*10^{-5}$) (Figure 2F).

In our previous study CD8$^+$ T cells were similarly clustered into two cellular states, one associated with activation and memory functions and the other with exhaustion.[29] Classifying samples based on the ratio between these immunological states achieved similar performance with AUC = 0.87. However, the R^2 between the previous predictor and the current metabolic one is 0.55 (Figure 2G), suggesting that the latter provides additional information. Indeed, a few samples that were misclassified as responders by the immunological predictor due to a high abundance of memory and activated CD8$^+$ T cells, were correctly classified using the metabolic predictor as non-responders (Figures 2H and S5). This set also includes non-responding samples which had a mutation in the β_2 microglobulin gene, associated with immune evasion (Figure 2H). From a metabolic point of view, we found that nine out of these ten misclassified non-responding samples had a high abundance (30–70%) of CD8$^+$ T cells from cluster C4, showing a significant difference between the correctly and incorrectly classified non-responding samples (two-sided Wilcoxon rank sum p value = $4.98*10^{-5}$, Figure S5). While this metabolic cluster was not significantly associated with patient response, we were able to identify several marker genes that significantly differentiate between memory-activated CD8$^+$ T cells in the true responding samples and the nine samples wrongly classified as responders (Table S3). The most significantly up-regulated gene in the samples wrongly classified as responders is *CD38* (Figure 2I), a glycoprotein found on the cell surface of many immune cells and converts NAD$^+$ to cyclic ADP ribose (cADPR) and to ADP ribose (ADPR).[35,36] This gene is known to exert immunosuppressive effects through multiple mechanisms, among them is the depletion of NAD$^+$ from the tumor microenvironment which impairs T cell activation and differentiation.[37] This finding therefore highlights a sub-cellular state of activated and memory CD8$^+$ T cells that expresses *CD38* and is abundant in non-responding samples. Overall, our analysis identified a highly predictive metabolic score for classifying patients according to their response status, emphasizing the importance of cellular metabolism in determining patient response.

Metabolic programs predict response to checkpoint immunotherapy

To generalize these findings into a predictive model that can be used in other datasets, one of two approaches can be taken: in the first, clustering can be performed in each given dataset. However, it would be difficult to receive the exact same clustering solution. The second approach is to use top genes from the two clusters, thus identifying the predictive metabolic cellular states. This solution sets a challenge in this case as the main characterization of C3 was a general down-regulation of metabolic genes. To overcome this obstacle we took a different approach that goes beyond discrete cell clusters and identifies transcriptional metabolic programs that exist as continuous activity programs across and within different cell clusters. This was done by applying consensus non-negative matrix factorization (cNMF),[38] an approach that performs soft clustering and assigns each cell a gene expression program with a usage value ranging between 0 and 1. We identified ten different metabolic programs (Figure 3A, STAR Methods; Table S4), four of them are "identity programs" that are active in specific cell clusters, and the other six are "activity programs" that are active across different cell clusters (Figure 3A). Examining the association of the activity programs with patient response, we found that two of them, P2 and P6, are more abundant in responders and non-responders, respectively (two-sided Wilcoxon rank sum p values = 0.075 and $5.08*10^{-5}$, respectively, Figure 3B). As expected, at the single-cell level these two metabolic programs are also related to the identified C2 and C3 clusters, such that P2 is more abundant in C3 (two-sided Wilcoxon rank sum p value = $4.37*10^{-130}$) and P6 in C2 (p value = $8.09*10^{-178}$, Figure 3C).

To examine the robustness of these programs we analyzed an additional scRNA-seq dataset from non-small cell lung cancer patients (NSCLC) treated with ICI.[39] Similar programs were identified using this dataset, with similar association with patient response (Figure S6; Table S4). Focusing on these two transcriptional programs, we found that P6 is enriched with OXPHOS (hypergeometric one-sided p value = $1.9*10^{-10}$), glycolysis (p value = $3.8*10^{-4}$) and purine synthesis (p value = 0.005), and P2 is enriched with inositol phosphate metabolism (p value = 0.012, Table S4, STAR Methods). Indeed, a previous report showed that high OXPHOS in a specific CD8$^+$ T cells subset is predictive of immunotherapy resistance in melanoma patients.[40]

Intersecting the gene markers of P2 and P6 between the two datasets, we assembled a narrowed list of the top metabolic markers (STAR Methods, Table S4). Following a robustness analysis (STAR Methods), we converged on the top 6 markers in each program. The first, P2, that we termed "Metabolic state A" contains *GSTK1, DGKA, LDHB, MGAT4A, NMRK1*, and *APRT*. The second, P6, that we termed "Metabolic state B" contains *PKM, ENO1, COX5A, COX6B1, NDUFB3*, and *COX8A*. While the second group clearly points to activation of glycolysis and OXPHOS, the first contains genes that are active across different metabolic pathways. However, we noticed that most exert known protective effect. Specifically, GSTK1 is a glutathione S-transferase that plays a role in cellular detoxification by conjugating reduced glutathione to electrophilic substrates.[41,42] LDHB converts lactate to pyruvate and by that reduces the acidity of the environment.[43,44] DGK deficient mice
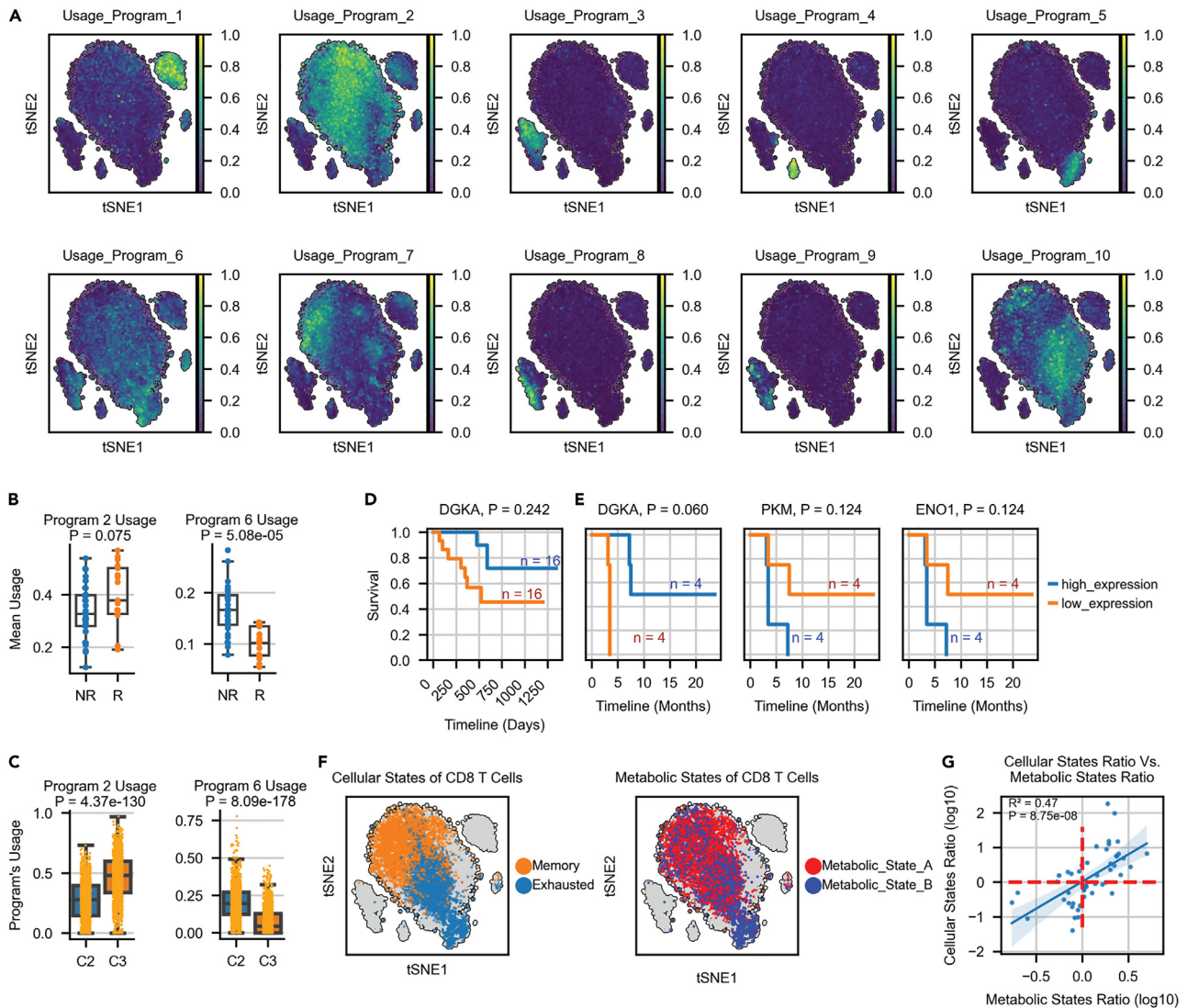
Figure 3. Metabolic programs predict response to checkpoint immunotherapy

(A) 10 metabolic programs obtained using cNMF.[38]

(B) Distribution of the mean usage values in programs P2 and P6, separated by the samples' response status. Wilcoxon rank sum test.

(C) The usage of programs P2 and P6 in the single-cell level of metabolic clusters C2 and C3. Wilcoxon rank sum test.

(D) The association of *DGKA* (as marker of program P2) with overall survival in melanoma[29] (n = 32). Logrank test.

(E) The association of *DGKA*, as well as the glycolytic genes *PKM* and *ENO1* (as markers of program P6) with progression free survival in triple-negative breast cancer[51] (TNBC, n = 8). Logrank test.

(F) Classification of CD8$^+$ T cells into major immunological cellular states, as previously determined[29] (left) and into major metabolic states (right) according to the top selected markers of each metabolic program.

(G) Spearman correlation between the metabolic score calculated as the ratio of CD8$^+$ T cells from metabolic states A and B in each sample vs. the predictive score suggested by Sade-Feldman et al.[29] Abbreviations: R = Responders, NR = Non-responders. See also Figure S6 and Table S4.

were shown to contain fewer antigen specific memory CD8$^+$ T cells after LCMV infection,[45] and NMRK1 synthesizes NAD$^+$ which is an important factor for T cell activation and differentiation.[46] MGAT4A is an N-acetylglucosaminyltransferase which attaches N-acetylglucosamine (GlcNAc) to the nitrogen atom of an asparagine side-chain, thus playing a crucial role in the regulation of many intracellular and extracellular functions.[47,48] It was also found to be differentially expressed in CD4$^+$ and CD8$^+$ tumor infiltrating memory T cells in melanoma patients.[49] In hepatocellular carcinoma patients (HCC), it was found to be downregulated in PD1^{high} tumor infiltrating CD8$^+$ T cells compared to PD1^{intermediate} CD8$^+$ T cells.[50] Here, we found that *MGAT4A* is differentially expressed in CD8$^+$ T cells from samples of responding melanoma patients (Figure 1F). Lastly, APRT is part of the nucleotide salvage pathway that converts adenine to AMP, and thus may contribute to cell proliferation. Examining the association of these genes with patient survival, we found that the expression of some of them clearly separates
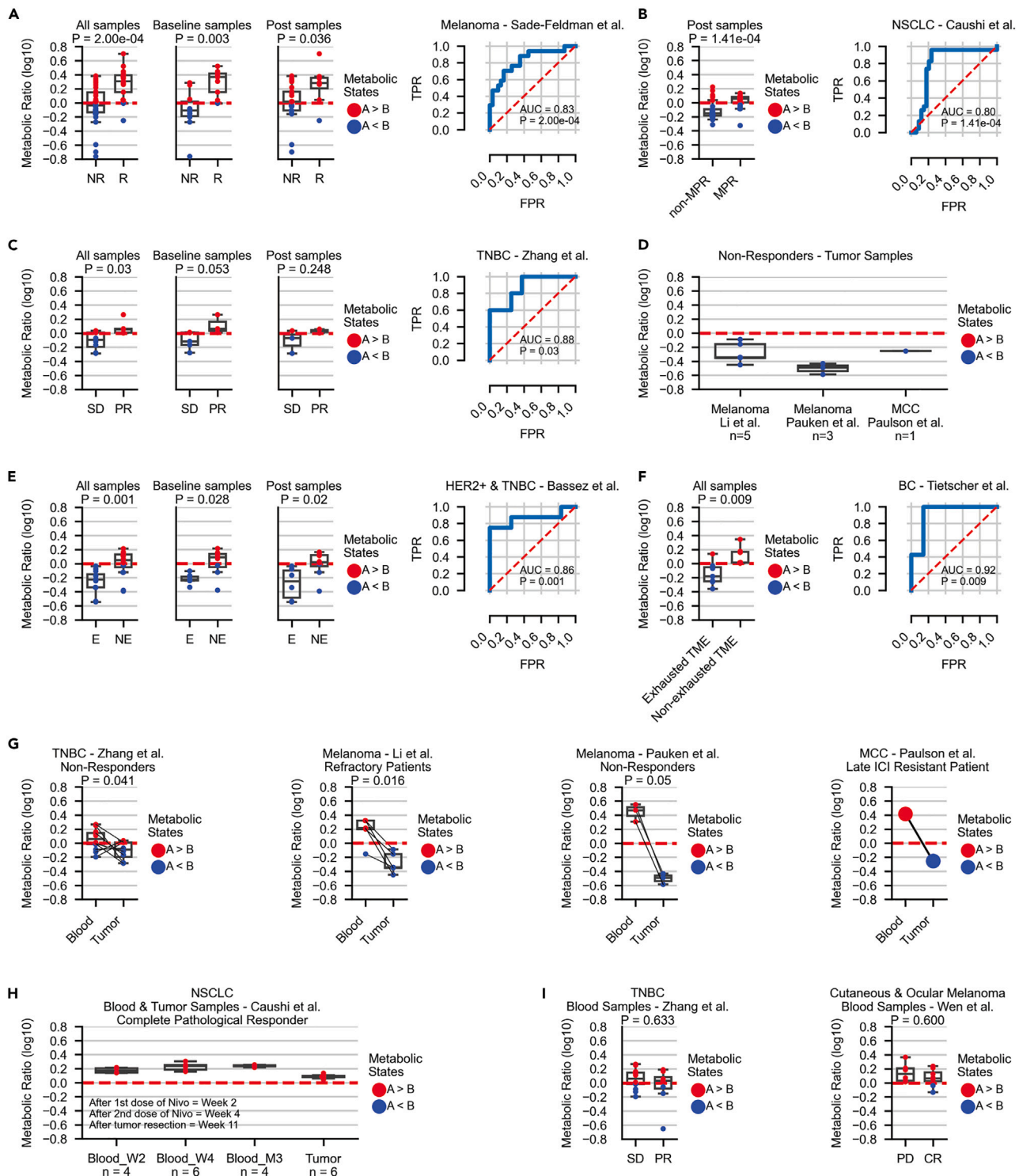
Figure 4. The predictive power of metabolic states across different datasets and cancer types in biopsies and blood samples

(A) The performance of the metabolic predictor in melanoma (n = 48).[29] ROC and the corresponding AUC achieved by the metabolic score are shown on the right; Distribution of the metabolic score in responders and non-responders in the different time points is shown on the left (n = 19 and 29 for pre and post treatment, respectively). Wilcoxon rank sum test.

(B) The performance of the metabolic predictor in NSCLC (n = 57, only post treatment samples).[39] ROC and the corresponding AUC achieved by the metabolic score are shown on the right; distribution of the metabolic score in responders and non-responders is shown on the left. Wilcoxon rank sum test.

Figure 4. Continued

(C) The performance of the metabolic predictor in triple negative breast cancer (TNBC, n = 13).[51] ROC and the corresponding AUC achieved by the metabolic score are shown on the right; distribution of the metabolic score in responders and non-responders in the different time points is shown on the left (n = 8 and 5 for pre and post treatment, respectively). Wilcoxon rank sum test.

(D) The metabolic states in four datasets including only non-responding patients from three studies, spanning melanoma[40,52] (n = 5,3 respectively) and MCC[53] (n = 1).

(E) The performance of the metabolic predictor in breast cancer samples having annotations for clonal expansion (n = 28).[54] ROC and the corresponding AUC achieved by the metabolic score are shown on the right; distribution of the metabolic score for the two annotated groups in the different time points is shown on the left (n = 14 and 14 for pre and post treatment, respectively). Wilcoxon rank sum test.

(F) The performance of the metabolic predictor in breast cancer dataset annotated by environmental exhaustion state (n = 14).[55] ROC and the corresponding AUC achieved by the metabolic score are shown on the right; distribution of the metabolic score for the different annotated groups is shown on the left. Wilcoxon rank sum test.

(G) A shift in the metabolic states of CD8$^+$ T cells in tumor samples and their matched blood samples taken from non-responding patients with TNBC[51] (8 pairs of tumor and their matched blood samples, with additional 6 unpaired blood samples), melanoma[40,52] (5 and 3 pairs, respectively), and MCC[53] (1 pair). Wilcoxon rank sum test.

(H) Similar metabolic states of CD8$^+$ T cells in blood samples (n = 14) and tumor samples (n = 6) of a single complete pathological responder having NSCLC.[39]

(I) Similar metabolic states of CD8$^+$ T cells in blood samples of responding and non-responding patients having TNBC[51] (n = 22) (left) and cutaneous and ocular melanoma[57] (n = 16) (right). Wilcoxon rank sum test. Abbreviations: R = Responders, NR = Non-responders, MPR = Major pathological response, SD = Stable disease, PR = Partial response, PD = Progressive disease, CR = Complete response, E = Clonal expansion, NE = No (or low) clonal expansion, TME = Tumor microenvironment. See also Figures S7–11, as well as Tables S1 and S4.

between patients, though the difference was not significant after correction for multiple hypotheses due to a relatively small sample size. We found that the expression of *DGKA* in CD8$^+$ T cells is associated with a longer overall survival in melanoma[29] (adjusted log rank p value = 0.242, Figure 3D) and a longer progression free survival (PFS) in triple-negative breast cancer (TNBC)[51] (adjusted log rank p value = 0.06, Figure 3E). On the other hand, *PKM* and *ENO1* were associated with shorter PFS in TNBC[51] (adjusted log rank p value = 0.124 for both genes, Figure 3E).

Based on the expression of these metabolic markers, we divided all CD8$^+$ T cells into two major groups of metabolic state A and B (Figure 3F, STAR Methods). We then classified samples as responders or non-responders based on the ratio between the number of cells associated with either of these two metabolic states (STAR Methods). Examining the correlation between this metabolic score and that achieved by our previous immunological one,[29] we found that it explains only 47% of the variance, emphasizing the added information captured by the metabolic classification (R^2 = 0.47, p value = 8.75*10^{-8}, Figure 3G). We first tested the predictive power of this metabolic score in the aforementioned melanoma and NSCLC datasets. In melanoma,[29] our predictor achieved an AUC of 0.83 (n = 48, p value = 2*10^{-4}, Figure 4A). A significant difference was maintained also when examining baseline and post-therapy samples separately (n = 19 and 29, p values = 0.003 and 0.036, respectively). In NSCLC containing only post-therapy samples,[39] our metabolic metric achieved an AUC of 0.8 (n = 57, p value = 1.41*10^{-4}, Figure 4B). These results, as well as the sensitivity and specificity measures, were robust to a different number of top markers (Figure S7; Table S4). Of note, shuffling the markers across single cells resulted in random results (STAR Methods), demonstrating that the existence or absence of these genes is mostly a biological rather than a technical result (Figure S8).

To further establish the robustness of this predictor, we analyzed seven additional datasets from the public domain having scRNA-seq data from patients treated with ICI.[40,51–55] In a TNBC dataset,[51] our predictor achieved an AUC of 0.88 (n = 13, p value = 0.03, Figure 4C). In three melanoma datasets (n = 8) and one MCC dataset (n = 1), all with only non-responding patients,[40,52,53] our predictor correctly classified all samples showing a greater number of CD8$^+$ T cells found in metabolic state B (Figure 4D). Importantly, our results remained significant also when separating patients according to the different ICI treatments (Figure S9). Next, we applied our predictor to a dataset of HER2 positive and TNBC patients annotated with a clonal expansion phenotype.[54] We found that samples enriched with metabolic state A are more abundant where no (or low) T cell expansion was observed, while metabolic state B was more abundant in samples with high clonal expansion (AUC = 0.86, n = 28, p value = 0.001, Figure 4E). This significant trend was observed also when examining baseline and post-therapy samples separately (n = 14 and 14, p values = 0.028 and 0.02, respectively, Figure 4E). These findings are in agreement with the authors' original findings that low clonal expansion is enriched in cells with a memory phenotype (*TCF7$^+$*, *GZMK$^+$*), while clonal expansion is enriched with cells expressing exhaustion markers (*HAVCR2*, *LAG3*, Figure S10). They also coincide with a study in melanoma patients showing that highly expanded clonotype families were distributed predominantly in cells with exhausted phenotype having decreased diversity of T cell receptors (TCRs).[56]

Finally, we applied our predictor to a dataset containing mostly treatment-naive breast cancer patients having a classification for exhausted and non-exhausted TME provided by the authors.[55] This classification is based on the presence or absence of *PD1^{high}/CTLA4^{high}/CD38^{high}* T cells. Our predictor achieved an AUC of 0.92 and significantly differentiated between these two tumor environmental states (n = 14, p value = 0.009, Figure 4F). Importantly, our metabolic predictor outperformed the predictor based on immunological cellular states[29] in all three breast cancer datasets analyzed in this study,[51,54,55] further demonstrating its importance (STAR Methods, Figure S11).

The metabolic states of blood peripheral CD8$^+$ T cells are non-predictive of patient response

Applying our metabolic classification to CD8$^+$ T cells from blood samples of seven different datasets,[39,40,51–53,57] spanning melanoma, NSCLC, TNBC, and MCC, we found that CD8$^+$ T cells in the blood are mostly found in metabolic state A, both in responders and non-responders. This finding corresponds with their general naive-bystander phenotype and lack of checkpoint genes expression. A shift in the metabolic states of CD8$^+$ T cells reflects this finding when comparing tumor samples and their matched blood samples taken from

non-responding patients with melanoma, TNBC, and MCC[40,51–53] (Figure 4G). Measuring the metabolic score in blood samples taken at different time points from an NSCLC patient experiencing a complete pathological response,[39] we observed similar ranges of scores as seen in blood samples of non-responding patients (Figure 4H). We also could not identify significant differences between the metabolic scores obtained from blood samples of responding and non-responding TNBC patients,[51] as well as cutaneous and ocular melanoma patients[57] (Figure 4I). These findings demonstrate that the metabolic state of CD8$^+$ T cells is mainly predictive within the TME and emphasize the challenge of identifying reliable blood-based biomarkers.

A metabolically distinct macrophage cluster in an acquired resistance patient

Clustering the immune cells using the metabolic genes subdivided the original macrophages/monocytes cluster into two metabolic clusters, C7 and C8 (Figure 2B). While all the metabolic clusters were evenly distributed across samples, 82% of the cells associated with C8 were of two specific biopsies (73% and 9%, respectively) from a patient developed acquired resistance following therapy[29] (Figure 5A). Considering known macrophages markers, we found that C7 cells have a higher expression of the RNA editing enzyme APOBEC3A and of interferon related genes such as IFITM1, ISG20, IFI44L and IDO1 (Table S3; Figure S12), typical to the pro-inflammatory classic macrophages and interferon-primed macrophages.[58,59] C8 cells have a higher expression of metallothionein genes such as MT1F, MT1X, MT1E and MT1G, corresponding to the alternatively activated anti-inflammatory macrophages,[60] together with lipid-related genes (APOE, APOC1, ACP5 and FABP5) corresponding to lipid-associated macrophages having canonical M2-like pathways.[58,61–63] Focusing on C8 that was highly enriched in the acquired resistance patient, we found a high expression of several genes in the heme degradation pathway. These include, HMOX1, HMOX2, BLVRA, and BLVRB (Table S3; Figure S12). Interestingly, it was previously shown in vitro and in animal models that HMOX1 is involved in the polarization of macrophages into the alternative M2-like phenotype.[64] Here, we identify these genes in this unique patient, suggesting a potential mechanism of resistance to ICI, and highlighting metabolic drug targets for enhancing treatment response.

We next analyzed the corresponding tumor sample of this patient, and compared it to 5 additional tumor samples available in this dataset that lack the M2-like signature[65] (Figure 5B, STAR Methods). We found a significant increase in the expression of CSF1, CCL2, and VEGFA (Fisher's exact test p values = $4.18*10^{-92}$, $1.04*10^{-29}$, and $5.78*10^{-68}$, respectively), all are tumor-derived factors associated with recruitment of macrophages to the TME and their polarization to the M2-like phenotype[66,67] (Figure 5B; Table S5). In addition, we identified a significantly higher expression of HIF1A (p value = $2.9*10^{-49}$) which is known to induce VEGFA secretion.[68] Considering the metabolic activity of this tumor sample, we found a significantly higher expression of fructose and mannose metabolism (hypergeometric one-sided p value = 0.027) and aminosugar metabolism (p value = 0.027, Figure 5C; Table S5, STAR Methods). This tumor also differentially expressed 50% of the genes related to glycolysis and additional genes related to sugar-uptake such as GLUT1 (SLC2A1) and GLUT3 (SLC2A3), compared to a maximum of 2 glycolytic genes in all other tumors (Figure 5B; Table S5). In addition, we observed a high expression of LDHA in all of these tumor cells, and of MCT4 (SLC16A3), an enzyme catalyzing the secretion of lactate, in 84% of the cells (Figure 5B; Table S5). This finding coincides with previous reports regarding the role of lactate in inducing the polarization of macrophages toward the pro-tumorigenic M2-like phenotype.[69,70] Overall, our findings highlight a specific mechanism of resistance involving a tumor with high activation of sugar-related pathways and its association with anti-inflammatory macrophages, which may be controlled, at least in part, by metabolic genes.

DISCUSSION

In this study, we utilized scRNA-seq data and performed an in-depth transcriptomic characterization of the metabolic changes that occur in immune cells found in the TME of patients treated with ICI. We found a general up-regulation of the metabolic activity in cell types associated with non-responding samples such as exhausted cycling cells, dendritic cells, and macrophages. On the other hand, we observed a general metabolic down-regulation in cell types associated with responding samples such as B cells and memory T cells. Re-clustering the data based on metabolic genes uncovered novel metabolic clusters associated with patient response, each is a mix of different known immunological cellular states. These clusters demonstrate that different immunological states can share metabolic similarity, while similar immunological states can vary in their metabolic properties. With more data becoming available, the transition between these metabolic states can be studied using TCR sequencing. Furthermore, we detected continuous metabolic programs with different activity levels across CD8$^+$ T cells. Utilizing the top genes of two key programs, we were able to accurately classify patients by their response status across various cancer types, including melanoma, MCC, lung, and breast cancers. Finally, we found that CD8$^+$ T cells in blood samples are mostly found in a single metabolic state, regardless of their response status.

An unsupervised analysis of scRNA-seq data typically includes the investigation of all genes passing a set of quality control criteria. This type of analysis naturally highlights the most significant signals found in the data. However, at the same time, it might miss important changes that are weaker and are lost due to multiple hypothesis correction. While this study is a re-analysis of published data, our semi-supervised analysis which was focused on the well-defined biological process of cellular metabolism, was able to uncover significant changes associated with patient response that were not detected in the previous genome-wide analyses done by us and others. We believe that these discoveries were made possible due to the importance of metabolism in immune cells function and interaction with tumor and other cells in the TME.

By identifying metabolic programs with various activity levels across cells, we were able to suggest a sub-classification of CD8$^+$ T cells that is predictive of patient response in different cancer types. Importantly, this metabolic-based classification provides additional information not captured by our original classification that was based on the ratio between the number of cells found in an activation\memory vs. exhausted cellular state.[29] This was found to be specifically crucial in breast cancer where the metabolic predictor achieved significantly improved results. It is therefore plausible that other cellular processes can form additional sub-classifications that will be predictive of patient response.
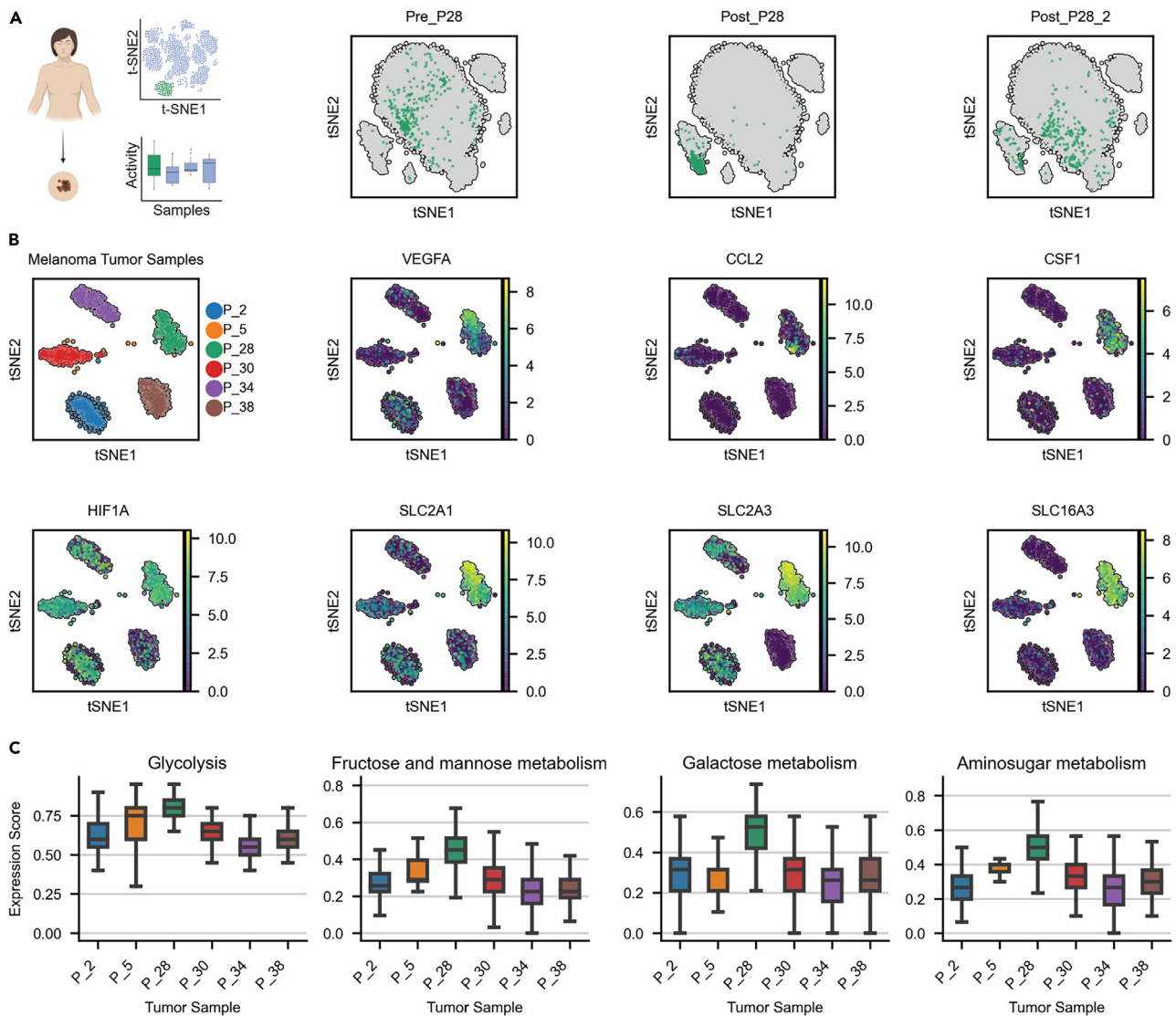
Figure 5. A metabolically distinct macrophage cluster in an acquired resistance patient

(A) Three biopsies obtained by a single acquired resistance patient (P28),[29] with two biopsies containing 73% and 9% respectively of the cells related to metabolic cluster C8.

(B) Six samples of CD45⁻ malignant cells[65] and selected differentially expressed genes in the tumor sample of the resistant patient.

(C) Metabolic score of sugar-related pathways across the different tumor samples. See also Figure S12 and Table S5.

Metabolism of immune cells has been widely studied, though mainly *in vitro* and in animal models. To the best of our knowledge, this is the first study that metabolically analyzed immune cells from cancer patients treated with ICI, supporting the importance of metabolic processes in determining patient response to therapy across different cancer types. Taken together, the increase in clinically annotated data of patients treated with ICI, and the accumulation of additional single-cell omics-data, is expected to significantly advance our understanding of immune cell metabolism and its role in patient response to ICI.

Limitations of the study

In order to fully understand cellular metabolic changes and aid biomarker identification, single-cell proteomic and metabolomic data should be collected and analyzed as well. While these technologies are rapidly advancing, they have not yet reached the scale of transcriptomic data.[71–73] Moreover, functional studies are required to determine the causal effects of metabolic changes on tumor and immune cellular states. In addition, since metabolism is a central process in all living cells, the set of metabolic marker genes found as predictive in our analysis, is also expressed in tumor cells (Figures S13 andS14). This makes it challenging to use bulk RNA-seq data for validation purposes.

Nonetheless, our findings provide an improved understanding of immune cell metabolism in the TME of ICI treated patients. Furthermore, the highlighted genes might be used for modifying T cell function through co-engineering strategies, thus improving T cells' metabolic fitness and augmenting tumor control of T cell therapies.[74] Finally, more data have to be collected in order to address potential links between blood-based metabolic biomarkers and the metabolic landscape of the TME. This could also include a possible connection between the predictive value of serum LDH levels,[75–79] and the secretion of lactate into the TME, which was discussed here as a plausible factor related to an acquired ICI-resistance.

STAR★METHODS

Detailed methods are provided in the online version of this paper and include the following:

- KEY RESOURCES TABLE
- RESOURCE AVAILABILITY
  - Lead contact
  - Materials availability
  - Data and code availability
- METHOD DETAILS
  - Single-cell RNA-seq datasets and preprocessing
  - Metabolic genes and metabolic pathways scores
  - Metabolic pathway activity and its association with patient response
  - Dimensionality reduction and unsupervised metabolic clustering of immune cells
  - Trajectory analysis of metabolic clusters
  - Differential expression analysis
  - Identifying metabolic programs
  - Pathway enrichment analysis
  - Identification of CD8$^+$ T cells
  - Testing data imputation for the selection of CD8$^+$ T cells
  - Reconstruction of the metabolic predictor
  - Testing a possible influence of dropouts on the presence of the selected metabolic markers
  - Survival analysis
  - Application of the cellular states predictor
  - Melanoma tumor analysis

SUPPLEMENTAL INFORMATION

Supplemental information can be found online at https://doi.org/10.1016/j.isci.2023.108188.

AUTHOR CONTRIBUTIONS

O.S. and K.Y. conceived the idea. O.S. and K.Y. designed the study. O.S. performed the analysis. O.S. and K.Y. wrote the manuscript.

DECLARATION OF INTERESTS

The authors declare no competing interests.

REFERENCES

1. Pardoll, D.M. (2012). The blockade of immune checkpoints in cancer immunotherapy. Nat. Rev. Cancer *12*, 252–264. https://doi.org/10.1038/nrc3239.

2. Fares, C.M., Van Allen, E.M., Drake, C.G., Allison, J.P., and Hu-Lieskovan, S. (2019). Mechanisms of Resistance to Immune Checkpoint Blockade: Why Does Checkpoint Inhibitor Immunotherapy Not Work for All Patients? Am. Soc. Clin. Oncol. Educ. Book. *39*, 147–164. https://doi.org/10.1200/edbk_240837.

3. Gauci, M.L., Lanoy, E., Champiat, S., Caramella, C., Ammari, S., Aspeslagh, S., Varga, A., Baldini, C., Bahleda, R., Gazzah, A., et al. (2019). Long-term survival in patients responding to anti-PD-1/PD-L1 therapy and disease outcome upon treatment discontinuation. Clin. Cancer Res. *25*, 946–956. https://doi.org/10.1158/1078-0432.CCR-18-0793.

4. Hargadon, K.M., Johnson, C.E., and Williams, C.J. (2018). Immune checkpoint blockade therapy for cancer: An overview of FDA-approved immune checkpoint inhibitors. Int. Immunopharm. *62*, 29–39. https://doi.org/10.1016/j.intimp.2018.06.001.

5. Pitt, J.M., Vétizou, M., Daillère, R., Roberti, M.P., Yamazaki, T., Routy, B., Lepage, P., Boneca, I.G., Chamaillard, M., Kroemer, G., and Zitvogel, L. (2016). Resistance Mechanisms to Immune-Checkpoint Blockade in Cancer: Tumor-Intrinsic and -Extrinsic Factors. Immunity *44*, 1255–1269. https://doi.org/10.1016/j.immuni.2016.06.001.

6. Ayers, M., Lunceford, J., Nebozhyn, M., Murphy, E., Loboda, A., Kaufman, D.R., Albright, A., Cheng, J.D., Kang, S.P., Shankaran, V., et al. (2017). IFN-γ-related mRNA profile predicts clinical response to PD-1 blockade. J. Clin. Invest. *127*, 2930–2940. https://doi.org/10.1172/JCI91190.

7. Prat, A., Navarro, A., Paré, L., Reguart, N., Galván, P., Pascual, T., Martínez, A., Nuciforo, P., Comerma, L., Alos, L., et al. (2017). Immune-Related Gene Expression Profiling After PD-1 Blockade in Non–Small Cell Lung Carcinoma, Head and Neck Squamous Cell Carcinoma, and Melanoma. Cancer Res. *77*, 3540–3550. https://doi.org/10.1158/0008-5472CAN-16-3556.

8. Riaz, N., Havel, J.J., Makarov, V., Desrichard, A., Urba, W.J., Sims, J.S., Hodi, F.S., Martín-Algarra, S., Mandal, R., Sharfman, W.H., et al. (2017). Tumor and Microenvironment Evolution during Immunotherapy with Nivolumab. Cell *171*, 934–949.e16. https://doi.org/10.1016/j.cell.2017.09.028.

9. Tumeh, P.C., Harview, C.L., Yearley, J.H., Shintaku, I.P., Taylor, E.J.M., Robert, L., Chmielowski, B., Spasic, M., Henry, G., Ciobanu, V., et al. (2014). PD-1 blockade induces responses by inhibiting adaptive immune resistance. Nature *515*, 568–571. https://doi.org/10.1038/nature13954.

10. Chen, P.-L., Roh, W., Reuben, A., Cooper, Z.A., Spencer, C.N., Prieto, P.A., Miller, J.P., Bassett, R.L., Gopalakrishnan, V., Wani, K., et al. (2016). Analysis of Immune Signatures in Longitudinal Tumor Samples Yields Insight into Biomarkers of Response and Mechanisms of Resistance to Immune Checkpoint Blockade. Cancer Discov. *6*, 827–837. https://doi.org/10.1158/2159-8290.CD-15-1545.

11. Daud, A.I., Loo, K., Pauli, M.L., Sanchez-Rodriguez, R., Sandoval, P.M., Taravati, K., Tsai, K., Nosrati, A., Nardo, L., Alvarado, M.D., et al. (2016). Tumor immune profiling predicts response to anti-PD-1 therapy in human melanoma. J. Clin. Invest. *126*, 3447–3452. https://doi.org/10.1172/JCI87324.

12. Van Allen, E.M., Miao, D., Schilling, B., Shukla, S.A., Blank, C., Zimmer, L., Sucker, A., Hillen, U., Foppen, M.H.G., Goldinger, S.M., et al. (2015). Genomic correlates of response to CTLA-4 blockade in metastatic melanoma. Science *350*, 207–211. https://doi.org/10.1126/science.aad0095.

13. Sade-Feldman, M., Jiao, Y.J., Chen, J.H., Rooney, M.S., Barzily-Rokni, M., Eliane, J.-P., Bjorgaard, S.L., Hammond, M.R., Vitzthum, H., Blackmon, S.M., et al. (2017). Resistance to checkpoint blockade therapy through inactivation of antigen presentation. Nat. Commun. *8*, 1136. https://doi.org/10.1038/s41467-017-01062-w.

14. Roh, W., Chen, P.-L., Reuben, A., Spencer, C.N., Prieto, P.A., Miller, J.P., Gopalakrishnan, V., Wang, F., Cooper, Z.A., Reddy, S.M., et al. (2017). Integrated molecular analysis of tumor biopsies on sequential CTLA-4 and PD-1 blockade reveals markers of response and resistance. Sci. Transl. Med. *9*, eaah3560. https://doi.org/10.1126/scitranslmed.aah3560.

15. Rizvi, N.A., Hellmann, M.D., Snyder, A., Kvistborg, P., Makarov, V., Havel, J.J., Lee, W., Yuan, J., Wong, P., Ho, T.S., et al. (2015). Mutational landscape determines sensitivity to PD-1 blockade in non–small cell lung cancer. Science *348*, 124–128. https://doi.org/10.1126/science.aaa1348.

16. Hellmann, M.D., Nathanson, T., Rizvi, H., Creelan, B.C., Sanchez-Vega, F., Ahuja, A., Ni, A., Novik, J.B., Mangarin, L.M.B., Abu-Akeel, M., et al. (2018). Genomic Features of Response to Combination Immunotherapy in Patients with Advanced Non-Small-Cell Lung Cancer. Cancer Cell *33*, 843–852.e4. https://doi.org/10.1016/j.ccell.2018.03.018.

17. Chang, C.H., and Pearce, E.L. (2016). Emerging concepts of T cell metabolism as a target of immunotherapy. Nat. Immunol. *17*, 364–368. https://doi.org/10.1038/ni.3415.

18. Renner, K., Singer, K., Koehl, G.E., Geissler, E.K., Peter, K., Siska, P.J., and Kreutz, M. (2017). Metabolic Hallmarks of Tumor and Immune Cells in the Tumor Microenvironment. Front. Immunol. *8*, 248. https://doi.org/10.3389/fimmu.2017.00248.

19. Chang, C.-H., Qiu, J., O'Sullivan, D., Buck, M.D., Noguchi, T., Curtis, J.D., Chen, Q., Gindin, M., Gubin, M.M., van der Windt, G.J.W., et al. (2015). Metabolic Competition in the Tumor Microenvironment Is a Driver of Cancer Progression. Cell *162*, 1229–1241. https://doi.org/10.1016/j.cell.2015.08.016.

20. Arner, E.N., and Rathmell, J.C. (2023). Metabolic programming and immune suppression in the tumor microenvironment. Cancer Cell *41*, 421–433. https://doi.org/10.1016/j.ccell.2023.01.009.

21. Guerra, L., Bonetti, L., and Brenner, D. (2020). Metabolic Modulation of Immunity: A New Concept in Cancer Immunotherapy. Cell Rep. *32*, 107848. https://doi.org/10.1016/j.celrep.2020.107848.

22. Fox, C.J., Hammerman, P.S., and Thompson, C.B. (2005). Fuel feeds function: Energy metabolism and the T-cell response. Nat. Rev. Immunol. *5*, 844–852. https://doi.org/10.1038/nri1710.

23. Liu, Y., Liang, X., Dong, W., Fang, Y., Lv, J., Zhang, T., Fiskesund, R., Xie, J., Liu, J., Yin, X., et al. (2018). Tumor-Repopulating Cells Induce PD-1 Expression in CD8+ T Cells by Transferring Kynurenine and AhR Activation. Cancer Cell *33*, 480–494.e7. https://doi.org/10.1016/j.ccell.2018.02.005.

24. Watson, M.J., Vignali, P.D.A., Mullett, S.J., Overacre-Delgoffe, A.E., Peralta, R.M., Grebinoski, S., Menk, A.V., Rittenhouse, N.L., DePeaux, K., Whetstone, R.D., et al. (2021). Metabolic support of tumour-infiltrating regulatory T cells by lactic acid. Nature *591*, 645–651. https://doi.org/10.1038/s41586-020-03045-2.

25. Brand, A., Singer, K., Koehl, G.E., Kolitzus, M., Schoenhammer, G., Thiel, A., Matos, C., Bruss, C., Klobuch, S., Peter, K., et al. (2016). LDHA-Associated Lactic Acid Production Blunts Tumor Immunosurveillance by T and NK Cells. Cell Metabol. *24*, 657–671. https://doi.org/10.1016/j.cmet.2016.08.011.

26. Fischer, K., Hoffmann, P., Voelkl, S., Meidenbauer, N., Ammer, J., Edinger, M., Gottfried, E., Schwarz, S., Rothe, G., Hoves, S., et al. (2007). Inhibitory effect of tumor cell-derived lactic acid on human T cells. Blood *109*, 3812–3819. https://doi.org/10.1182/blood-2006-07-035972.

27. Elia, I., Rowe, J.H., Johnson, S., Joshi, S., Notarangelo, G., Kurmi, K., Weiss, S., Freeman, G.J., Sharpe, A.H., and Haigis, M.C. (2022). Tumor cells dictate anti-tumor immune responses by altering pyruvate utilization and succinate signaling in CD8+ T cells. Cell Metabol. *34*, 1137–1150.e6. https://doi.org/10.1016/j.cmet.2022.06.008.

28. Thiele, I., Swainston, N., Fleming, R.M.T., Hoppe, A., Sahoo, S., Aurich, M.K., Haraldsdottir, H., Mo, M.L., Rolfsson, O., Stobbe, M.D., et al. (2013). A community-driven global reconstruction of human metabolism. Nat. Biotechnol. *31*, 419–425. https://doi.org/10.1038/nbt.2488.

29. Sade-Feldman, M., Yizhak, K., Bjorgaard, S.L., Ray, J.P., de Boer, C.G., Jenkins, R.W., Lieb, D.J., Chen, J.H., Frederick, D.T., Barzily-Rokni, M., et al. (2018). Defining T Cell States Associated with Response to Checkpoint Immunotherapy in Melanoma. Cell *175*, 998–1013.e20. https://doi.org/10.1016/j.cell.2018.10.038.

30. Eisenhauer, E.A., Therasse, P., Bogaerts, J., Schwartz, L.H., Sargent, D., Ford, R., Dancey, J., Arbuck, S., Gwyther, S., Mooney, M., et al. (2009). New response evaluation criteria in solid tumours: Revised RECIST guideline (version 1.1). Eur. J. Cancer *45*, 228–247. https://doi.org/10.1016/j.ejca.2008.10.026.

31. Xiao, Z., Dai, Z., and Locasale, J.W. (2019). Metabolic landscape of the tumor microenvironment at single cell resolution. Nat. Commun. *10*, 3763–3812. https://doi.org/10.1038/s41467-019-11738-0.

32. Zhang, C., Wang, Y., Wang, F., Wang, Z., Lu, Y., Xu, Y., Wang, K., Shen, H., Yang, P., Li, S., et al. (2017). Quantitative profiling of glycerophospholipids during mouse and human macrophage differentiation using targeted mass spectrometry. Sci. Rep. *7*, 412–413. https://doi.org/10.1038/s41598-017-00341-2.

33. Robichaud, P.P., Boulay, K., Munganyiki, J.É., and Surette, M.E. (2013). Fatty acid remodeling in cellular glycerophospholipids

following the activation of human T cells. J. Lipid Res. *54*, 2665–2677. https://doi.org/10.1194/jlr.M037044.

34. Collison, L.W., Murphy, E.J., and Jolly, C.A. (2008). Glycerol-3-phosphate acyltransferase-1 regulates murine T-lymphocyte proliferation and cytokine production. Am. J. Physiol. Cell Physiol. *295*, 1543–1549. https://doi.org/10.1152/ajpcell.00371.2007.

35. Chini, E.N. (2009). CD38 as a Regulator of Cellular NAD: A Novel Potential Pharmacological Target for Metabolic Conditions. Curr. Pharmaceut. Des. *15*, 57–63. https://doi.org/10.2174/138161209787185788.

36. Aksoy, P., White, T.A., Thompson, M., and Chini, E.N. (2006). Regulation of intracellular levels of NAD: A novel role for CD38. Biochem. Biophys. Res. Commun. *345*, 1386–1392. https://doi.org/10.1016/j.bbrc.2006.05.042.

37. Kar, A., Mehrotra, S., and Chatterjee, S. (2020). CD38: T Cell Immuno-Metabolic Modulator. Cells *9*, 1716. https://doi.org/10.3390/cells9071716.

38. Kotliar, D., Veres, A., Nagy, M.A., Tabrizi, S., Hodis, E., Melton, D.A., and Sabeti, P.C. (2019). Identifying gene expression programs of cell-type identity and cellular activity with single-cell RNA-Seq. Elife *8*, e43803. https://doi.org/10.7554/eLife.43803.

39. Caushi, J.X., Zhang, J., Ji, Z., Vaghasia, A., Zhang, B., Hsiue, E.H.C., Mog, B.J., Hou, W., Justesen, S., Blosser, R., et al. (2021). Transcriptional Programs of Neoantigen-specific TIL in Anti-PD-1-treated Lung Cancers (Springer US). https://doi.org/10.1038/s41586-021-03752-4.

40. Li, C., Phoon, Y.P., Karlinsey, K., Tian, Y.F., Thapaliya, S., Thongkum, A., Qu, L., Matz, A.J., Cameron, M., Cameron, C., et al. (2022). A high OXPHOS CD8 T cell subset is predictive of immunotherapy resistance in melanoma patients. J. Exp. Med. *219*, e20202084. https://doi.org/10.1084/jem.20202084.

41. Singh, R.R., and Reindl, K.M. (2021). Glutathione S-Transferases in Cancer. https://doi.org/10.3390/antiox10050701.

42. Chatterjee, A., and Gupta, S. (2018). The multifaceted role of glutathione S-transferases in cancer. Cancer Lett. *433*, 33–42. https://doi.org/10.1016/j.canlet.2018.06.028.

43. Wang, Z.H., Peng, W.B., Zhang, P., Yang, X.P., and Zhou, Q. (2021). Lactate in the tumour microenvironment: From immune modulation to therapy. EBioMedicine *73*, 103627. https://doi.org/10.1016/j.ebiom.2021.103627.

44. Decking, S.M., Bruss, C., Babl, N., Bittner, S., Klobuch, S., Thomas, S., Feuerer, M., Hoffmann, P., Dettmer, K., Oefner, P.J., et al. (2022). LDHB Overexpression Can Partially Overcome T Cell Inhibition by Lactic Acid. Int. J. Mol. Sci. *23*, 5970. https://doi.org/10.3390/ijms23115970.

45. Shin, J., O'Brien, T.F., Grayson, J.M., and Zhong, X.-P. (2012). Differential Regulation of Primary and Memory CD8 T Cell Immune Responses by Diacylglycerol Kinases. J. Immunol. *188*, 2111–2117. https://doi.org/10.4049/jimmunol.1102265.

46. Ratajczak, J., Joffraud, M., Trammell, S.A.J., Ras, R., Canela, N., Boutant, M., Kulkarni, S.S., Rodrigues, M., Redpath, P., Migaud, M.E., et al. (2016). NRK1 controls nicotinamide mononucleotide and nicotinamide riboside metabolism in mammalian cells. Nat. Commun. *7*, 13103–13112. https://doi.org/10.1038/ncomms13103.

47. Reily, C., Stewart, T.J., Renfrow, M.B., and Novak, J. (2019). Glycosylation in health and disease. Nat. Rev. Nephrol. *15*, 346–366. https://doi.org/10.1038/s41581-019-0129-4.

48. Lau, K.S., Partridge, E.A., Grigorian, A., Silvescu, C.I., Reinhold, V.N., Demetriou, M., and Dennis, J.W. (2007). Complex N-Glycan Number and Degree of Branching Cooperate to Regulate Cell Proliferation and Differentiation. Cell *129*, 123–134. https://doi.org/10.1016/j.cell.2007.01.049.

49. Li, H., van der Leun, A.M., Yofe, I., Lubling, Y., Gelbard-Solodkin, D., van Akkooi, A.C.J., van den Braber, M., Rozeman, E.A., Haanen, J.B.A.G., Blank, C.U., et al. (2019). Dysfunctional CD8 T Cells Form a Proliferative, Dynamically Regulated Compartment within Human Melanoma. Cell *176*, 775–789.e18. https://doi.org/10.1016/j.cell.2018.11.043.

50. Kim, H.D., Song, G.W., Park, S., Jung, M.K., Kim, M.H., Kang, H.J., Yoo, C., Yi, K., Kim, K.H., Eo, S., et al. (2018). Association Between Expression Level of PD1 by Tumor-Infiltrating CD8+ T Cells and Features of Hepatocellular Carcinoma. Gastroenterology *155*, 1936–1950.e17. https://doi.org/10.1053/j.gastro.2018.08.030.

51. Zhang, Y., Chen, H., Mo, H., Hu, X., Gao, R., Zhao, Y., Liu, B., Niu, L., Sun, X., Yu, X., et al. (2021). Single-cell analyses reveal key immune cell subsets associated with response to PD-L1 blockade in triple-negative breast cancer. Cancer Cell *39*, 1578–1593.e8. https://doi.org/10.1016/j.ccell.2021.09.010.

52. Pauken, K.E., Shahid, O., Lagattuta, K.A., Mahuron, K.M., Luber, J.M., Lowe, M.M., Huang, L., Delaney, C., Long, J.M., Fung, M.E., et al. (2021). Single-cell analyses identify circulating anti-tumor CD8 T cells and markers for their enrichment. J. Exp. Med. *218*, e20200920. https://doi.org/10.1084/JEM.20200920.

53. Paulson, K.G., Voillet, V., McAfee, M.S., Hunter, D.S., Wagener, F.D., Perdicchio, M., Valente, W.J., Koelle, S.J., Church, C.D., Vandeven, N., et al. (2018). Acquired cancer resistance to combination immunotherapy from transcriptional loss of class I HLA. Nat. Commun. *9*, 3868. https://doi.org/10.1038/s41467-018-06300-3.

54. Bassez, A., Vos, H., Van Dyck, L., Floris, G., Arijs, I., Desmedt, C., Boeckx, B., Vanden Bempt, M., Nevelsteen, I., Lambein, K., et al. (2021). A single-cell map of intratumoral changes during anti-PD1 treatment of patients with breast cancer. Nat. Med. *27*, 820–832. https://doi.org/10.1038/s41591-021-01323-8.

55. Tietscher, S., Wagner, J., Anzeneder, T., Langwieder, C., Rees, M., Sobottka, B., de Souza, N., and Bodenmiller, B. (2023). A comprehensive single-cell map of T cell exhaustion-associated immune environments in human breast cancer. Nat. Commun. *14*, 98. https://doi.org/10.1038/s41467-022-35238-w.

56. Oliveira, G., Stromhaug, K., Klaeger, S., Kula, T., Frederick, D.T., Le, P.M., Forman, J., Huang, T., Li, S., Zhang, W., et al. (2021). Phenotype, specificity and avidity of antitumour CD8+ T cells in melanoma. Nature *596*, 119–125. https://doi.org/10.1038/s41586-021-03704-y.

57. Wen, T., Barham, W., Li, Y., Zhang, H., Gicobi, J.K., Hirdler, J.B., Liu, X., Ham, H., Peterson Martinez, K.E., Lucien, F., et al. (2022). NKG7 Is a T-cell-Intrinsic Therapeutic Target for Improving Antitumor Cytotoxicity and Cancer Immunotherapy. Cancer Immunol. Res. *10*, 162–181. https://doi.org/10.1158/2326-6066.CIR-21-0539.

58. Ma, R.Y., Black, A., and Qian, B.Z. (2022). Macrophage diversity in cancer revisited in the era of single-cell omics. Trends Immunol. *43*, 546–563. https://doi.org/10.1016/j.it.2022.04.008.

59. Alqassim, E.Y., Sharma, S., Khan, A.N.M.N.H., Emmons, T.R., Cortes Gomez, E., Alahmari, A., Singel, K.L., Mark, J., Davidson, B.A., Robert McGray, A.J., et al. (2021). RNA editing enzyme APOBEC3A promotes pro-inflammatory M1 macrophage polarization. Commun. Biol. *4*, 102–111. https://doi.org/10.1038/s42003-020-01620-x.

60. Chowdhury, D., Alrefai, H., Landero Figueroa, J.A., Candor, K., Porollo, A., Fecher, R., Divanovic, S., Deepe, G.S., and Subramanian Vignesh, K. (2019). Metallothionein 3 Controls the Phenotype and Metabolic Programming of Alternatively Activated Macrophages. Cell Rep. *27*, 3873–3886.e7. https://doi.org/10.1016/j.celrep.2019.05.093.

61. Zheng, P., Luo, Q., Wang, W., Li, J., Wang, T., Wang, P., Chen, L., Zhang, P., Chen, H., Liu, Y., et al. (2018). Tumor-associated macrophages-derived exosomes promote the migration of gastric cancer cells by transfer of functional Apolipoprotein e. Cell Death Dis. *9*, 434. https://doi.org/10.1038/s41419-018-0465-5.

62. Baitsch, D., Bock, H.H., Engel, T., Telgmann, R., Müller-Tidow, C., Varga, G., Bot, M., Herz, J., Robenek, H., Von Eckardstein, A., and Nofer, J.R. (2011). Apolipoprotein e induces antiinflammatory phenotype in macrophages. Arterioscler. Thromb. Vasc. Biol. *31*, 1160–1168. https://doi.org/10.1161/ATVBAHA.111.222745.

63. Hao, X., Zheng, Z., Liu, H., Zhang, Y., Kang, J., Kong, X., Rong, D., Sun, G., Sun, G., Liu, L., et al. (2022). Inhibition of APOC1 promotes the transformation of M2 into M1 macrophages via the ferroptosis pathway and enhances anti-PD1 immunotherapy in hepatocellular carcinoma based on single-cell RNA sequencing. Redox Biol. *56*, 102463. https://doi.org/10.1016/j.redox.2022.102463.

64. Naito, Y., Takagi, T., and Higashimura, Y. (2014). Heme oxygenase-1 and anti-inflammatory M2 macrophages. Arch. Biochem. Biophys. *564*, 83–88. https://doi.org/10.1016/j.abb.2014.09.005.

65. Mehta, A., Rucevic, M., Sprecher, E., Hacohen, N., Boland, G., Parikh, M., Chen, J., Frederick, D., Woods, E., Bi, L., et al. (2022). 150 Circulatory plasma proteomic biomarkers predict response to immunotherapy in melanoma patients and reveal biological insights into the tumor microenvironment. J. Immunother. Cancer *10*. A163 LP-A163. https://doi.org/10.1136/jitc-2022-SITC2022.0150.

66. Lin, Y., Xu, J., and Lan, H. (2019). Tumor-associated macrophages in tumor metastasis: Biological roles and clinical therapeutic applications. J. Hematol. Oncol. *12*, 76. https://doi.org/10.1186/s13045-019-0760-3.

67. Zhu, S., Yi, M., Wu, Y., Dong, B., and Wu, K. (2021). Roles of tumor-associated macrophages in tumor progression: implications on therapeutic strategies. Exp. Hematol. Oncol. *10*, 60. https://doi.org/10.1186/s40164-021-00252-z.

68. Hashimoto, T., and Shibasaki, F. (2015). Hypoxia-Inducible Factor as an Angiogenic Master Switch. Front. Pediatr. 3, 33. https://doi.org/10.3389/fped.2015.00033.

69. Colegio, O.R., Chu, N.Q., Szabo, A.L., Chu, T., Rhebergen, A.M., Jairam, V., Cyrus, N., Brokowski, C.E., Eisenbarth, S.C., Phillips, G.M., et al. (2014). Functional polarization of tumour-associated macrophages by tumour-derived lactic acid. Nature 513, 559–563. https://doi.org/10.1038/nature13490.

70. Qian, Y., Galan-Cobo, A., Guijarro, I., Dang, M., Molkentine, D., Poteete, A., Zhang, F., Wang, Q., Wang, J., Parra, E., et al. (2023). MCT4-dependent lactate secretion suppresses antitumor immunity in LKB1-deficient lung adenocarcinoma. Cancer Cell 41, 1363–1380.e7. https://doi.org/10.1016/j.ccell.2023.05.015.

71. Lanekoff, I., Sharma, V.V., and Marques, C. (2022). Single-cell metabolomics: where are we and where are we going? Curr. Opin. Biotechnol. 75, 102693–102697. https://doi.org/10.1016/j.copbio.2022.102693.

72. Seydel, C. (2021). Single-cell metabolomics hits its stride. Nat. Methods 18, 1452–1456. https://doi.org/10.1038/s41592-021-01333-x.

73. Bennett, H.M., Stephenson, W., Rose, C.M., and Darmanis, S. (2023). Single-cell proteomics enabled by next-generation sequencing or mass spectrometry. Nat. Methods 20, 363–374. https://doi.org/10.1038/s41592-023-01791-5.

74. Giordano Attianese, G.M.P., Ash, S., and Irving, M. (2023). Coengineering specificity, safety, and function into T cells for cancer immunotherapy. Immunol. Rev. 1–33. https://doi.org/10.1111/imr.13252.

75. Xu, J., Zhao, J., Wang, J., Sun, C., and Zhu, X. (2021). Prognostic value of lactate dehydrogenase for melanoma patients receiving anti-PD-1/PD-L1 therapy: A meta-analysis. Méd. 100, E25318. https://doi.org/10.1097/MD.0000000000025318.

76. Tjokrowidjaja, A., Lord, S.J., John, T., Lewis, C.R., Kok, P.S., Marschner, I.C., and Lee, C.K. (2022). Pre- and on-treatment lactate dehydrogenase as a prognostic and predictive biomarker in advanced non–small cell lung cancer. Cancer 128, 1574–1583. https://doi.org/10.1002/cncr.34113.

77. Li, Y., Wang, K., Zhao, E., Li, B., Li, S., Dong, X., Yuan, L., and Yang, H. (2022). Prognostic Value of Lactate Dehydrogenase in Second-Line Immunotherapy for Advanced Esophageal Squamous Cell Carcinoma. Pathol. Oncol. Res. 28, 1610245. https://doi.org/10.3389/pore.2022.1610245.

78. Van Wilpe, S., Koornstra, R., Den Brok, M., De Groot, J.W., Blank, C., De Vries, J., Gerritsen, W., and Mehra, N. (2020). Lactate dehydrogenase: a marker of diminished antitumor immunity. OncoImmunology 9, 1731942. https://doi.org/10.1080/2162402X.2020.1731942.

79. Diem, S., Kasenda, B., Spain, L., Martin-Liberal, J., Marconcini, R., Gore, M., and Larkin, J. (2016). Serum lactate dehydrogenase as an early marker for outcome in patients treated with anti-PD-1 therapy in metastatic melanoma. Br. J. Cancer 114, 256–261. https://doi.org/10.1038/bjc.2015.467.

80. Benjamini, Y., and Hochberg, Y. (1995). Controlling the False Discovery Rate: A Practical and Powerful Approach to Multiple Testing. J. R. Stat. Soc. Ser. B 57, 289–300.

81. Brunk, E., Sahoo, S., Zielinski, D.C., Altunkaya, A., Dräger, A., Mih, N., Gatto, F., Nilsson, A., Preciat Gonzalez, G.A., Aurich, M.K., et al. (2018). Recon3D: A resource enabling a three-dimensional view of gene variation in Human metabolism. Nat. Biotechnol. 36, 272–281. https://doi.org/10.1038/nbt.4072.Recon3D.

82. Maaten, L.V.D., and Hinton, G. (2008). Visualizing Data using t-SNE, 9, pp. 2579–2605. https://lvdmaaten.github.io/tsne/.

83. Wolf, F.A., Angerer, P., and Theis, F.J. (2018). SCANPY: large-scale single-cell gene expression data analysis. Genome Biol. 19, 15. https://doi.org/10.1186/s13059-017-1382-0.

84. Traag, V.A., Waltman, L., and van Eck, N.J. (2019). From Louvain to Leiden: guaranteeing well-connected communities. Sci. Rep. 9, 5233–5312. https://doi.org/10.1038/s41598-019-41695-z.

85. Cao, J., Spielmann, M., Qiu, X., Huang, X., Ibrahim, D.M., Hill, A.J., Zhang, F., Mundlos, S., Christiansen, L., Steemers, F.J., et al. (2019). The single-cell transcriptional landscape of mammalian organogenesis. Nature 566, 496–502. https://doi.org/10.1038/s41586-019-0969-x.

86. Eraslan, G., Simon, L.M., Mircea, M., Mueller, N.S., and Theis, F.J. (2019). Single-cell RNA-seq denoising using a deep count autoencoder. Nat. Commun. 10, 390–414. https://doi.org/10.1038/s41467-018-07931-2.

87. Tickle, T., Tirosh, I., Georgescu, C., Brown, M., and Haas, B. (2019). inferCNV of the Trinity CTAT Project (Klarman Cell Obs. Broad Inst. MIT Harvard). https://github.com/broadinstitute/inferCNV.

88. RR Core Team (2019). A Language and Environment for Statistical Computing (R Found. Stat. Comput.). https://www.R-project.org.

STAR★METHODS

KEY RESOURCES TABLE

REAGENT or RESOURCE	SOURCE	IDENTIFIER
Deposited data		
Single-cell RNA sequencing data - Melanoma	Sade-Feldman et al.[29]	GEO: GSE120575
Single-cell RNA sequencing data - NSCLC	Caushi et al.[39]	GEO: GSE176021
Single-cell RNA sequencing data - TNBC	Zhang et al.[51]	GEO: GSE169246
Single-cell RNA sequencing data - BC	Bassez et al.[54]	https://lambrechtslab.sites.vib.be/en
Single-cell RNA sequencing data - BC	Tietscher et al.[55]	ArrayExpress: E-MTAB-10607
Single-cell RNA sequencing data - Melanoma	Li et al.[40]	GEO: GSE138720
Single-cell RNA sequencing data - Melanoma	Li et al.[40]	GEO: GSE153098
Single-cell RNA sequencing data - Melanoma	Pauken et al.[52]	GEO: GSE159251
Single-cell RNA sequencing data - MCC	Paulson et al.[53]	GEO: GSE118056
Single-cell RNA sequencing data - Melanoma	Wen et al.[57]	GEO: GSE164237
Software and algorithms		
Python version 3.8.8	Python Software Foundation	https://www.python.org/
Scanpy version 1.8.2	Wolf et al.[83]	https://github.com/scverse/scanpy
Leiden clustering algorithm	Traag et al.[84]	https://github.com/vtraag/leidenalg
tSNE	Maaten and Hinton[82]	https://lvdmaaten.github.io/tsne/
cNMF version 1.3.2	Kotliar et al.[38]	https://github.com/dylkot/cNMF
R version 4.1.1	R Core Team[88]	https://www.r-project.org/
InferCNV version 1.2.1	Tickle et al.[87]	https://github.com/broadinstitute/infercnv
Monocle3 version 1.0.0	Cao et al.[85]	https://cole-trapnell-lab.github.io/monocle3/
Deep Count Auto-encoder (DCA) version 0.3.4	Eraslan et al.[86]	https://github.com/theislab/dca

RESOURCE AVAILABILITY

Lead contact

Further information and requests for resources should be directed to and will be fulfilled by the lead contact, Keren Yizhak (kyizhak@technion.ac.il).

Materials availability

This study did not generate new unique reagents.

Data and code availability

- This paper analyzes existing, publicly available data. These accession numbers for the datasets are listed in the key resources table and are summarized in Table S1.
- This paper does not report original code.
- Any additional information required to reanalyze the data reported in this paper is available from the lead contact upon request.

METHOD DETAILS

Single-cell RNA-seq datasets and preprocessing

We used 10 scRNA-seq datasets,[29,39,40,51–55,57] with six of them containing tumor biopsies with their matched blood samples, three with only tumor biopsies, and one dataset containing only blood samples (Table S1). Expression levels for the single smart-seq2 dataset that we have previously published[29] were quantified as transcripts per million (TPM). All other datasets were droplet-based and contained read counts. Expression levels in these cases were first normalized to a standard sum of 10,000 reads per cell, and then log transformed as follows: $\log_2(normalized\_counts + 1)$. It should be noted though that the per-cell read coverage in these datasets is larger than 10,000. Only samples with defined clinical annotations (response or clonal expansion) were included in the analysis. Furthermore, we considered only patients that

were treated with either ICI or a combination of ICI and chemo, as well as a single Merkel cell carcinoma patient that was treated with a combination of T cell therapy and ICI.[53] Our analysis also included a pair of patients having ocular melanoma.[57] The first received a combination of ICI and Indoximod, while the second was administered a combination of ICI, radiotherapy and microwave ablation. We also used a dataset of a non-ICI cohort containing mostly treatment-naive patients having annotations for exhausted and-non exhausted TME provided by the authors[55] (Table S1).

Metabolic genes and metabolic pathways scores

The set of metabolic genes and pathways used in the analysis is based on the Recon 2 metabolic reconstruction.[28] We used the set of 1689 metabolic genes that were expressed in Sade-Feldman et al.[29] (Table S2). The glycolysis pathway as defined in Recon 2 is composed of 78 genes and includes also the gluconeogenesis-related genes. Therefore, to specifically study glycolysis in our analysis, we defined a "Glycolysis" pathway which includes only 20 central genes (Table S2). To compute a metabolic pathway score for each pathway in every single cell, we calculated for every cell the amount of expressed genes related to each metabolic pathway, out of the total number of genes in that pathway, yielding a continuous ratio between 0 and 1 for each pathway in each cell. Specifically, for each metabolic pathway K, the metabolic pathway score of a single cell was calculated such that:

$$P_k = \frac{\sum_{j=1}^{n_k} is\_expressed(gene_j)}{n_k}$$

Where $is\_expressed : x \rightarrow \{0, 1\}$ and defined as:

$$is\_expressed(x) := \begin{cases} 1 & if \log_2(x+1) > 2.5 \\ 0 & if \log_2(x+1) \leq 2.5 \end{cases}$$

x is the expression level in TPM units, n_k is the total number of genes in metabolic pathway K, and the sum is applied on all of the genes such that $gene_j \in pathway_k$.

Metabolic pathway activity and its association with patient response

In order to characterize the metabolic activity of different cell types, we averaged the metabolic pathway scores described above across all cells of each immune cell type. We also ranked the general activity of each metabolic pathway by the mean score of that pathway across all single cells.

To identify metabolic genes that are differentially expressed between responding and non-responding samples, we calculated for every sample the percentage of cells expressing that gene in the two response groups. We included only genes with median expression fraction higher than 5% across all samples and conducted a two-sided Wilcoxon rank sum test between the two groups. We then corrected the obtained P-values for multiple hypothesis using the Benjamini-Hochberg false discovery rate.[80] We considered corrected P-values < 0.05 as significant and repeated that process focusing only on CD8$^+$ T cells (Table S3). To identify metabolic pathways that are differentially expressed between responding and non-responding samples, we calculated the mean score of each metabolic pathway in each sample and repeated the statistical analysis described above. We conducted this analysis using all cell types and CD8$^+$ T cells separately (Table S3).

Dimensionality reduction and unsupervised metabolic clustering of immune cells

Principle component analysis (PCA) was applied to all CD45$^+$ cells in Sade-Feldman et al.,[29] using 3580 metabolic genes obtained from Recon 3D[81] (Table S2). The top 50 components obtained by the PCA were used for the downstream t-distributed stochastic neighbor embedding (tSNE)[82] with Scanpy's[83] default perplexity parameter of 30, learning rate of 1,000 and the Euclidean distance metric. The reason we used Recon 3D genes here is that they also contain signaling and regulatory genes, generating a more clear 2D visualization. Importantly, the tSNE algorithm was used only for visualization and was not part of the clustering analysis described below.

To identify cell clusters based on metabolic processes we used Scanpy's neighbors function with 1689 metabolic enzymes from Recon 2[28], and generated the K nearest-neighbors (KNN) graph. We then applied the Leiden algorithm[84] with the default parameters implemented in Scanpy, yielding 10 different metabolic clusters of immune cells (Table S3). To identify metabolic clusters that are significantly associated with patient response, we calculated for every metabolic cluster the fraction of cells assigned to that cluster in every sample. We then conducted a two-sided Wilcoxon rank sum test between these fractions in responders and non-responders. This process was done for each metabolic cluster and corrected for multiple hypothesis using the Benjamini-Hochberg false discovery rate.[80] Adjusted P-values < 0.05 were considered as significant. We repeated this analysis separately for the set of CD8$^+$ T cells.

Trajectory analysis of metabolic clusters

We conducted trajectory analysis using Monocle3 pseudo-time analysis[85] (https://github.com/cole-trapnell-lab/monocle3), applied on the set of metabolic genes as an input (Figure S4). This analysis was done for the five central adjacent metabolic clusters identified by our analysis, i.e. clusters C1-4, C6.

Differential expression analysis

In order to identify differentially expressed genes between two groups G_1 and G_2, we first considered only genes that are expressed $(\log_2(TPM + 1) > 2.5)$ in more than 10% of the cells, in at least one cluster. Following, for each gene i we count the number of cells in G_1 and G_2 that express it with an expression level $(\log_2(TPM + 1) > 2.5)$ or $(\log_2(TPM + 1) \leq 2.5)$. We then applied Fisher's Exact test for the corresponding 2x2 contingency table. Significant genes were those with an adjusted P-value < 0.05 after correcting for multiple hypothesis using the Benjamini-Hochberg false discovery rate[80] and $\log_2(FoldChange) > 0.5$. The set of differentially expressed genes in each cluster is listed in Table S3. This analysis was done to identify gene markers in each cluster, comparing it to all other clusters. We repeated this analysis separately, comparing C2 vs. C3, as well as C7 vs. C8.

Identifying metabolic programs

To identify metabolic programs we applied cNMF[38] on the raw counts matrix of the melanoma dataset by Sade-Feldman et al.,[29] with the set of 1689 metabolic genes. We filtered out immune cells with total of zero counts and neglected metabolic genes that were expressed in less than three cells. We used 200 NMF replicates for each K and tested the results for K = 5,…,20. Considering the error and stability values for each K, we selected K = 13 as the optimal solution. Further reviewing this solution, we filtered out three programs that were active (considering the max usage value) in less than 0.5% of the cells, leaving us with 10 metabolic programs overall. The same process was applied to the NSCLC dataset,[39] obtaining a final set of six programs. Normalized usage values and gene ranks for each program are summarized in Table S4. To identify metabolic programs that significantly differentiate between responding and non-responding samples, we first calculated the mean usage of each program across all CD8$^+$ T cells within each sample, while excluding programs having median of the mean usage lower than 0.1 across all samples. We performed a two-sided Wilcoxon rank sum test using the mean usage value of all CD8$^+$ T cells within each sample. This process was done for each metabolic program separately and P-values were adjusted using the Benjamini-Hochberg false discovery rate.[80] We considered adjusted P-values < 0.1 as significant for the melanoma dataset, and P-values < 0.15 as significant for the NSCLC dataset. For the melanoma dataset, this process yielded two significant programs (P2 and P6). For the NSCLC dataset, this process resulted with three significant programs (P2, P4 and P6), with the last two having 66% and 33% overlap with the melanoma programs P6 and P2, respectively, considering the top 100 genes in each program.

Pathway enrichment analysis

To identify enriched metabolic pathways, we applied a hypergeometric test for each metabolic pathway using the following probability mass function:

$$p(x, M, n, N) = \frac{\binom{n}{x} \cdot \binom{M - n}{N - x}}{\binom{M}{N}}$$

Where M is the effective domain size of all of the 1689 metabolic genes, N is the number of genes in the tested list of genes, n is the total number of genes associated with each metabolic pathway, and x is the number of genes from the tested metabolic pathway found in the tested list of genes. We calculated one-sided P-value for every metabolic pathway using:

$$1 - hypergeom.cdf(x - 1, M, n, N)$$

Where $hypergeom.cdf$ is the hypergeometric cumulative distribution function implemented by Scipy package version 1.6.2 in Python. We corrected multiple hypothesis using the Benjamini-Hochberg false discovery rate[80] and considered pathways with adjusted P-value < 0.05 as significant.

This analysis was done using the lists of the differentially expressed genes of metabolic clusters C2, C3, C7 and C8, and is described in Table S3. To identify enriched metabolic pathways in P2 and P6 of the melanoma dataset,[29] we applied this hypergeometric test for each metabolic pathway using the top 100 genes associated with each program, with N = 100 accordingly. The results of this analysis are summarized in Table S4.

Identification of CD8$^+$ T cells

In our previously published melanoma dataset we used the original classification of CD8$^+$ T cells that was based both on gene markers and manual curation.[29] In all of the other public datasets we used a stringent criteria such that a CD8$^+$ T cell must express *PTPRC* (*CD45*), *CD3E* and *CD8A* or *CD8B*, and cannot express either *NCR1*, *NCAM1* or *FOXP3*.[29] For these datasets a gene was considered as "expressed" if $\log_2(normalized\_counts + 1) > 1$, and "not expressed" otherwise. In all breast cancer datasets of Bassez et al.,[54] Zhang et al.,[51] and Tietscher et al.,[55] we did this process only after focusing on T cells according to the original cell type classification provided by the authors. In the NSCLC dataset of Caushi et al.,[39] we extracted CD8$^+$ T cells out of all of the sequenced cells as they went through CD3 positive cell filtration by flow cytometry. In the melanoma datasets of Li et al.,[40] Pauken et al.,[52] and Wen et al.,[57] we extracted CD8$^+$ T cells out of all of the sequenced cells as they went through CD8 positive filtration by flow cytometry. Finally, for the Merkel Cell Carcinoma dataset of Paulson et al.,[53] we extracted CD8$^+$ T cells out of all unsorted sequenced cells.

Testing data imputation for the selection of CD8+ T cells

Using a Deep Count Auto-encoder (DCA) for data imputation implemented in Scanpy,[83,86] we first fitted a density curve to the log2-transformed imputed *CD8A* expression values of all cells from all samples, using the optimize.curve_fit() function implemented by the Scipy library in Python. We then used the expression cut-off according to Caushi et al.[39]: "*as the trough of the bimodal density curve (that is, the first location where the first derivative is zero and the second derivative is positive)*".

An example of the bimodal distribution fitted to the imputed *CD8A* expression in the metastatic melanoma dataset by Sade-Feldman et al.[29] is displayed in Figure S15, including the imputed expression threshold (blue dashed line).

We used the imputed expression threshold of *CD8A* for the selection of CD8+ T cells as was done by Caushi et al.[39] In Figure S16, we show the selected CD8+ T cells according to our stringent inclusion criteria conducted using the non-imputed expression matrix vs. the selection using the imputed expression matrix, including various non-CD8 markers for reference. Setting higher thresholds for the imputed expression of *CD8A*, still resulted with CD8+ T cells having non-CD8 markers.

Reconstruction of the metabolic predictor

To reconstruct the metabolic predictor, we considered the two programs that were significantly associated with patient response and had a large overlap between the melanoma and NSCLC datasets.[29,39] In each dataset, genes of the two programs were first ranked according to their usage value. We then calculated the joint rank for the respective programs in both datasets and removed the single gene in each program that corresponded to a housekeeping gene (*RPL14* and *GAPDH*). We eventually selected the top K genes within each program for the reconstruction of the metabolic predictor (Table S4). We scored each CD8+ T cell based on the number of expressed genes out of the K 'Metabolic state A' markers and the K 'Metabolic state B' markers, yielding two scores for each CD8+ T cell. Then, each CD8+ T cell was classified as A or B based on the majority vote of the two scores: $n_{state\_A\_markers} \geq n_{state\_B\_markers}$ for A, and $n_{state\_A\_markers} < n_{state\_B\_markers}$ for B. Finally, we computed a score per sample by taking the ratio between the number of cells classified as belonging to 'Metabolic state A' and those belonging to 'Metabolic state B'. CD8+ T cells demonstrating an expression of zero markers from both lists of markers were excluded from this analysis. Samples with a ratio > 1 were classified as responders, and those with a ratio $\leq$ 1 were classified as non-responders. We performed this process on several datasets containing both response groups[29,39,51,54,55] for different values of K, ranging 3,...,25. For each K we calculated the Receiver Operating Curve (ROC) and the Area Under the Curve (AUC) score, as well as the sensitivity and specificity measures. Best results were achieved for K = 5,6 (Figure S7; Table S4). For simplicity, we selected K = 6 for all downstream analysis. A two-sided Wilcoxon rank sum test was used to calculate the P-value for the performance of the predictor, comparing the metabolic ratio score between true responders and non-responders. For the dataset of Bassez et al.,[54] we conducted this statistical test for the performance of the predictor between samples undergone clonal expansion and those with no (or low) clonal expansion. For the dataset of Tietscher et al.,[55] we compared between samples defined with exhausted TME and those with non-exhausted TME, provided by the authors.

Testing a possible influence of dropouts on the presence of the selected metabolic markers

Two different approaches were taken in order to address a possible influence of dropouts on the presence of the metabolic markers selected in this study.

In the first, we used the imputed expression values of each metabolic marker in every CD8+ T cell. Several markers (out of the chosen 12) didn't demonstrate a bimodal density curve of their imputed expression values, making it not trivial to point a certain threshold of expression in their unimodal representation (Figure S17). In a case where a marker had a unimodal representation, the threshold was determined based on visual inspection and empirical considerations. The performance of our predictor using the imputed expression values is demonstrated in Figure S18.

For the second approach, we used the non-imputed data and randomly shuffled the expression of the metabolic markers across all CD8+ T cells in two ways:

a. We first permutated all of the metabolic markers, where each marker was shuffled separately across the cells.
b. We permutated the entire vector of markers across the cells where the vector of markers itself remained intact within each single-cell.

The purpose of this experiment is to show that the lack of marker expression in a given cell, is mostly a biological rather than a technical phenomenon (Figure S8).

Survival analysis

Two datasets in our analysis contained survival data.[29,51] For these two, we performed survival analysis examining whether any of the 12 genes used by our predictor are significantly associated with patient survival. As described above, only the set of CD8+ T cells was used in this analysis. For the melanoma dataset,[29] in cases where more than one sample was available for a single patient, we considered only the baseline sample, yielding 32 samples from 32 patients overall. Similarly, for the TNBC dataset[51] we considered only samples at baseline, yielding 8 samples overall. For each sample we first computed the mean expression of each gene across all of the associated CD8+ T cells. We then split the samples into two groups using the median gene expression value, and conducted logrank test between the two groups. P-values were corrected for multiple hypothesis using the Benjamini-Hochberg false discovery rate.[80] This process was conducted in each group of six markers (for metabolic states A and B) separately.

Application of the cellular states predictor

For each one of the three breast cancer datasets utilized in this study,[51,54,55] we calculated for each CD8$^+$ T cell identified by the pipeline described above, the fraction of the expressed memory-activated markers and that of the exhaustion markers provided by Sade-Feldman et al.[29] We then classified each CD8$^+$ T cell into one of two cellular states: memory-activated or exhausted, according to the higher fraction of expressed markers. For each sample we calculated the ratio of CD8$^+$ T cells from these two cellular states and examined the predictive power of this ratio, predicting samples as responders if the ratio of memory-activated/exhausted CD8$^+$ T cells was higher than 1, and the opposite for classification for negative response (Figure S11).

Melanoma tumor analysis

We utilized seven CD45$^-$ samples from 6 patients available in the melanoma dataset.[65] To identify the malignant cells we applied InferCNV[87] (https://github.com/broadinstitute/inferCNV/) using R software,[88] and marked those showing copy number variation patterns. We found that all samples had more than 350 malignant cells (out of 384 sequenced cells) except for P5 which had only 24 malignant cells and P28_2 which had only one malignant cell and therefore was combined with the malignant cells from her other available sample. We normalized the TPM matrix as described above and focused on the previously described 1689 metabolic genes. Differentially expressed genes and enriched metabolic pathways were identified in each tumor according to the pipeline described above (Table S5). tSNE[82] was applied using the set of 1689 metabolic genes for visualization. For each cell, we scored four sugar-related metabolic pathways as described above: "Glycolysis", "Fructose and mannose metabolism", "Aminosugar metabolism", and "Galactose metabolism".